

# AN EXTENSIVE NUMERICAL SURVEY OF THE CORRELATION BETWEEN OUTFLOW DYNAMICS AND ACCRETION DISK MAGNETIZATION

DENISS STEPANOV<sup>1</sup> AND CHRISTIAN FENDT

Max Planck Institute for Astronomy, Königstuhl 17, D-69117 Heidelberg, Germany

*Draft version April 26, 2016*

## ABSTRACT

We investigate the accretion-ejection process of jets from magnetized accretion disks. We apply a novel approach to the jet-launching problem in order to obtain correlations between the physical properties of the jet and the underlying disk. We extend and confirm the previous works of Tzeferacos et al. (2009) and Murphy et al. (2010) by scanning a large parameter range for the disk magnetization,  $\mu_D = 10^{-3.5} \dots 10^{-0.7}$ . We disentangle the disk magnetization at the foot point of the outflow as the main parameter that governs the properties of the outflow. We show how the four jet integrals known from steady-state MHD are correlated to the disk magnetization at the jet foot point. This agrees with the usual findings of the steady-state theory, however, here we obtain these correlations from time-dependent simulations that include the dynamical evolution of the disk in the treatment. In particular, we obtain robust correlations between the local disk magnetization and (i) the outflow velocity, (ii) the jet mass loading, (iii) jet angular momentum, and (iv) the local mass accretion rate. Essentially we find that strongly magnetized disks launch more energetic and faster jets, and, due to a larger Alfvén lever arm, these jets extract more angular momentum from the underlying disk. These kind of disk-jet systems have, however, a smaller mass loading parameter and a lower mass ejection-to-accretion ratio. The jets are launched at the disk surface where the magnetization is  $\mu(r, z) \simeq 0.1$ . The magnetization rapidly increases vertically providing the energy reservoir for subsequent jet acceleration. We find indication for a critical disk magnetization  $\mu_D \simeq 0.01$  that separates the regimes of magnetocentrifugally-driven and magnetic pressure-driven jets.

*Subject headings:* accretion, accretion disks – MHD – ISM: jets and outflows – stars: mass loss – stars: pre-main sequence galaxies: jets

## 1. INTRODUCTION

Astrophysical jets consist of magnetized material moving as highly collimated beams with high velocity. These outflows are typically bipolar in nature and are an ubiquitous phenomenon in a variety of astrophysical sources. Today it seems to be commonly accepted that jets and outflows are launched from a magnetized accretion disk surrounding a central object (Pudritz et al. 2007; Ray et al. 2007; Hawley et al. 2015).

A good number of studies have been devoted to the understanding of the launching process, i.e. the *transition from accretion to ejection*. These studies consider steady-state MHD (see e.g. Wardle & Königl 1993; Li 1995; Ferreira & Pelletier 1995; Königl et al. 2010; Salmeron et al. 2011) or time-dependent numerical simulations (see e.g. Kudoh et al. 1998; Casse & Keppens 2002, 2004; Meliani et al. 2006; Zanni et al. 2007; Tzeferacos et al. 2009; Murphy et al. 2010; Sheikheezami et al. 2012; Fendt & Sheikheezami 2013). Recent works consider the accretion-ejection evolution for long time scales and on a large computational grid (Stepanovs & Fendt 2014) and jet-launching by a large-scale magnetic field self-generated by a mean-field disk dynamo (Stepanovs et al. 2014), and also the non-axisymmetric launching process of disk jets (Sheikheezami & Fendt 2015). However, despite all the

efforts over decades, the fundamental question of what kind of disks drive jets and what kind of disks do not, is still not answered.

An essential ingredient for jet launching is a strong poloidal magnetic field, as shown by seminal analytical papers (Blandford & Payne 1982; Pudritz & Norman 1983; Uchida & Shibata 1984; Ferreira 1997), and further confirmed by numerical simulations (Uchida & Shibata 1985; Ustyugova et al. 1995; Ouyed & Pudritz 1997; Kudoh et al. 1998; Kato et al. 1998; Casse & Keppens 2002; Fendt & Čemeljić 2002; Zanni et al. 2007).

How the accretion disk magnetization affects the jet launching has been studied in detail by Tzeferacos et al. (2009) and Murphy et al. (2010). In Tzeferacos et al. (2009) no disk viscosity was included and angular momentum transfer was purely magnetic. These simulations confirmed earlier analytical works (e.g. Ferreira & Pelletier 1995) suggesting that only a large - near equipartition - magnetization is able to produce steady-state super fast magneto sonic jets. The simulations of Murphy et al. (2010) included disk viscosity and thus also viscous angular momentum transport. These authors showed - surprisingly - that also a weak disk magnetization could launch super-fast jets. The results were interpreted in the framework of *warm* disk wind solutions (Casse & Ferreira 2000), suggesting that numerical mass diffusion may exist that could mimic heating and physical mass diffusion. The acceleration of the material loaded onto the jet is achieved in the usual Blandford-Payne magneto-centrifugal as long as the jet magnetiza-

fendt@mpia.de

<sup>1</sup> Fellow of the *International Max Planck Research School for Astronomy and Cosmic Physics at the University of Heidelberg (IMPRS-HD)*

tion (the ratio of Poynting flux to kinetic energy flux) is larger than unity. In this case, also super-fast jet velocities could be obtained. The authors derived two main criteria for jet launching from their study. One is that the disk magnetization cannot be too small, as the jet magnetization is proportional to the disk magnetization. The other is that the diffusive process of mass loading that brings mass from the zone of resistive MHD (disk) to the zone of ideal MHD (jet) needs to be efficient.

It was further suggested that super fast magnetosonic jets can only be launched from disk surface areas where the magnetization  $\mu \sim B_p^2/P$  becomes about unity. That area seems to be concentrated to about 5 inner disk radii.

Sheikhnezami et al. (2012) and Fendt & Sheikhnezami (2013) report a variation of the disk Alfvén speed by a factor ten during their simulations. Usually the disk magnetic diffusivity prescription is parameterized by the Alfvén speed. Therefore, besides the magnetization, also the disk diffusivity is substantially modified during the simulations - a fact that severely affects the disk evolution and also the mass loading from the disk into the outflow.

Murphy et al. (2010) and Sheikhnezami et al. (2012) find outflows also from weakly magnetized disks. Sheikhnezami et al. (2012) conclude that the driving of these outflows was not in the regime of the magnetocentrifugal Blandford-Payne mechanism, but in the regime of a magnetic pressure-driven tower outflow. In Stepanovs & Fendt (2014) (hereafter paper I), we have demonstrated in more detail that it is essential to relate the *actual*<sup>2</sup> jet properties to the *actual* disk properties, as both disk and jet evolve dynamically in time. Thus, the initial simulation parameters such as the initial magnetization, do not necessarily characterize the jet evolution, as these parameters are substantially changing during the disk evolution.

In the present paper, we continue to investigate the correlation between disk magnetization and jet launching by applying a new approach based on the long-term evolution of the disk-jet system. We take advantage from the fact that due to the loss of disk mass by accretion and ejection, the disk physics slowly changes in time. However, each time interval of the evolution can be considered as a quasi steady state. By comparing the disk and jet parameters at *different times* - thus *snapshots* of the accretion-ejection structure at different times - we effectively compare the jet launching conditions of *different disks*.

Our new simulations extend those presented in paper I, allowing us to probe a broad parameter space concerning the disk magnetization. As a result, we will present numerical correlations between the disk magnetization and typical outflow parameters over a wide range of disk magnetization.

In Section 2 we introduce to our general model approach, in particular our approach to analyze the slowly evolving the disk-jet system. In Section 3 we present our model setup, the choice of parameters, and discuss the general evolution of the system (summarizing paper I in this point). In Section 4 we discuss physical properties of

the jet by introducing the jet steady-state MHD integrals and show how to derive them from our numerical simulations. In Section 5 we connect the disk magnetization to various jet properties and present general correlations between them. In Section 6 we discuss the relevance for the jet ejection mechanism and compare our results to other studies, mainly to the paper of Murphy et al. (2010). We summarize our results in Section 7.

## 2. GENERAL MODEL APPROACH

Before we detail our model setup, we summarize our approach of addressing the jet-launching problem for a range of disk magnetizations, thereby mentioning several key points. The novelty of our approach lies in the fact that *we take advantage of the long-term disk evolution*, mainly triggered by the disk mass loss during the simulation. This enables us to compare *different disks* of different magnetization.

We perform *large-scale simulations* which ignores the microphysics of the accretion disk. This approach allows us to evolve both the accretion disk and the jet extending far from the disk in the same computational domain. The drawback is that the peculiar realm of the disk turbulence enters the equations only as an effective profile of the magnetic diffusivity.

We further note that the magnetic diffusivity profile follows the standard prescription used in the literature (Zanni et al. 2007; Murphy et al. 2010), thus assuming a simple parameterization of the magnetic diffusivity strength by the diffusivity parameter  $\alpha_m$ . However, we keep the diffusivity scale height constant in time.

We summarize the essential of our approach in linking the disk quantities to the outflow quantities as follows:

- (1) We start a simulation with a certain initial disk magnetization and strength of the magnetic diffusivity.

- (2) As the accretion-ejection structure evolves in time a quasi-steady state is reached at which advection and diffusion balance.

- (3) Since the disk slowly loses mass to the central object and into the outflow, the disk magnetization slowly changes in time. This time scale can be estimated to 10,000 time units. We decided to show the simulation results at 10,000 time units for the purpose of this paper, although most simulations run longer.

- (4) As a consequence also the outflow characteristics change slowly in time.

- (5) We continuously measure the disk magnetization and the outflow parameters, both suitably averaged at certain radius and altitude along the outflow. This provides us with a time series of the actual magnetization and actual outflow parameters at a certain time.

- (6) Combining the actual physical properties for a certain time, we can then provide correlations between these physical properties - in particular, we will relate the outflow physical properties to the disk magnetization.

- (7) We may then interrelate the outflow parameters that result from the simulation to the asymptotic jet parameters by using the steady-state MHD integrals. This is possible since the slow disk evolution in quasi-steady state that takes much longer than the outflow propagation times scale that is the Keplerian time scale at the foot point of the outflow.

Since the disk magnetization and also the outflow parameters vary in time, we obtain a general correlation

<sup>2</sup> With “actual” we denote the conditions at a certain time, thus snapshots in time of the set of physical parameters.

between the disk magnetization and the outflow properties. In principle, such correlations can be obtained for a range of magnetic field foot point radii along the disk. However, as the evolution of the outer disk proceeds considerably slower, it is rather difficult to probe a broad range of magnetization at these radii.

### 3. MODEL SETUP

We apply the MHD code PLUTO (Mignone et al. 2007), version 4.0, solving the time-dependent, resistive MHD equations on a spherical grid  $(R, \theta)$ . We refer to  $(r, z)$  as cylindrical coordinates.

The code numerically solves for the mass conservation,

$$\frac{\partial \rho}{\partial t} + \nabla \cdot (\rho \mathbf{V}) = 0, \quad (1)$$

with the plasma density  $\rho$  and flow velocity  $\mathbf{V}$ , the momentum conservation,

$$\frac{\partial \rho \mathbf{V}}{\partial t} + \nabla \cdot \left[ \rho \mathbf{V} \mathbf{V} + \left( P + \frac{\mathbf{B} \cdot \mathbf{B}}{2} \right) \mathbf{I} - \mathbf{B} \mathbf{B} \right] + \rho \nabla \Phi_g = 0 \quad (2)$$

with the thermal pressure  $P$  and the magnetic field  $\mathbf{B}$ . We consider a central object of point mass  $M$  with the gravitational potential  $\Phi_g = -GM/R$  with the gravitational constant  $G$ . Note that equations are written in non-dimensional form, and as usual the factor  $4\pi$  is neglected for the magnetic field. We apply a polytropic equation of state,  $P \propto \rho^\gamma$ , with  $\gamma = 5/3$ .

The code further solves for the conservation of energy,

$$\begin{aligned} \frac{\partial e}{\partial t} + \nabla \cdot \left[ \left( e + P + \frac{\mathbf{B} \cdot \mathbf{B}}{2} \right) \mathbf{V} - (\mathbf{V} \cdot \mathbf{B}) \mathbf{B} + \bar{\eta} \mathbf{J} \times \mathbf{B} \right] \\ = -\Lambda_{\text{cool}}, \end{aligned} \quad (3)$$

with the total energy density,

$$e = \frac{P}{\gamma - 1} + \frac{\rho \mathbf{V} \cdot \mathbf{V}}{2} + \frac{\mathbf{B} \cdot \mathbf{B}}{2} + \rho \Phi_g, \quad (4)$$

given by the sum of thermal, kinetic, magnetic, and gravitational energy, respectively. The electric current density is denoted by  $\mathbf{J} = \nabla \times \mathbf{B}$ . As shown by Tzeferacos et al. (2013), cooling may indeed play a role for jet launching, influencing both jet density and velocity. For the sake of simplicity we set the cooling term equal to Ohmic heating,  $\Lambda_{\text{cool}} = -\bar{\eta} \mathbf{J} \cdot \mathbf{J}$ . Thus all generated heat is instantly radiated away.

The magnetic field evolution is governed by the induction equation

$$\frac{\partial \mathbf{B}}{\partial t} = \nabla \times (\mathbf{V} \times \mathbf{B} - \bar{\eta} \mathbf{J}), \quad (5)$$

In general the magnetic diffusivity is defined as a tensor,  $\bar{\eta}$ . We assume the diffusivity tensor to be diagonal with the non-zero components  $\eta_{\phi\phi} \equiv \eta_p$ , and  $\eta_{rr} = \eta_{zz} \equiv \eta_\phi$ , where we denote  $\eta_p$  as the *poloidal magnetic diffusivity*, and  $\eta_\phi$  as the toroidal magnetic diffusivity, respectively (see Sect. 3.2. and Sheikhnezami et al. 2012 and Fendt & Sheikhnezami 2013).

We normalize the system of equation as follows. Lengths are given in units of the inner disk radius  $R_0$ . Velocities are given in units of  $V_{K,0}$ , corresponding to the Keplerian speed at the inner radius. The time unit

is  $T_0 = R_0/V_{K,0}$ , which we call the *dynamical time step*. The time  $2\pi T_0 = 2\pi R_0/V_{K,0}$  corresponds to one revolution at the inner disk radius. Densities are given in units of  $\rho_0$ , the disk density at the inner radius at the disk midplane. For further details, in particular the astrophysical scaling, we refer to paper I.

We apply a numerical grid with equidistant spacing in  $\theta$ -direction, but stretched cell sizes in radial direction, considering  $\Delta R = R\Delta\theta$ . Our computational domain of a size  $R = (1, 1500R_0)$ ,  $\theta = (0, \pi/2)$  is discretized with  $(N_R \times N_\theta)$  grid cells. We use a general resolution of  $N_\theta = 128$ . In order to cover a factor 1500 in radius, we apply  $N_R = 600$ . This gives a resolution of 16 cells per disk height ( $2\epsilon$ ) in the general case. However, we have also performed a resolution study applying a resolution twice high (or low, respectively), thus using  $256 \times 1200$  (or  $64 \times 300$ ) cells for the whole domain, or 35 (9) cells per disk height (see paper I).

We select the Harten-Lax-van Leer (HLL) Riemann solver together with a third-order Runge-Kutta scheme for time evolution and the PPM (piecewise parabolic method) reconstruction of (Colella & Woodward 1984) for spatial integration. The magnetic field evolution follows the method of Constrained Transport (Londrillo & del Zanna 2004).

#### 3.1. Initial conditions

For the initial conditions we follow a standard setup, commonly used in the literature (Zanni et al. 2007; Sheikhnezami et al. 2012; Fendt & Sheikhnezami 2013), and further detailed in paper I. The initial structure of the accretion disk is calculated from the steady state force equilibrium,

$$\nabla P + \rho \nabla \Phi_g - \mathbf{J} \times \mathbf{B} - \frac{1}{R} \rho V_\phi^2 (\mathbf{e}_R \sin \theta + \mathbf{e}_\theta \cos \theta) = 0. \quad (6)$$

We solve these equations assuming radial self-similarity (see paper I).

An essential non-dimensional parameter governing the initial disk structure is the ratio  $\epsilon$  between the isothermal sound speed  $C_s^T = \sqrt{P/\rho}$  and the Keplerian velocity  $V_K = \sqrt{GM/r}$ , evaluated at the disk midplane,  $\epsilon \equiv [C_s^T/V_K]_{\theta=\pi/2}$ . This quantity determines the disk thermal scale height  $H_T = \epsilon r$ . We assume  $\epsilon = 0.1$  initially<sup>3</sup> The thermal disk height  $H_T$  will change during the disk evolution, however, it is not further used as a parameter. In contrast, we define a geometrical disk height, namely the scale length where disk density and rotation significantly decrease,  $H \equiv 2\epsilon r$ . This parameter remains fixed in time, and is used to define the initial condition and the vertical profile of the magnetic diffusivity (see Sect. 3.3).

Following Zanni et al. (2007), our reference simulation is initialized with a poloidal magnetic field only. This is defined by the 3-component of the vector potential with  $\mathbf{B} = \nabla \times A \mathbf{e}_\phi$ ,

$$A = \frac{4}{3} B_{p,0} R^{-1/4} \frac{m^{5/4}}{(m^2 + ctg^2\theta)^{5/8}}. \quad (7)$$

<sup>3</sup> Note that for the rest of the paper, when discussing the dynamical properties of disk and outflow, we consider the *adiabatic sound speed*  $C_s = \sqrt{\gamma P/\rho}$ .

The parameter  $B_{p,0}$  determines the strength of the initial magnetic field. The parameter  $m$  determines the degree of curvature of the poloidal magnetic field lines. As we have shown in paper I, the long-term evolution of the disk-jet structure is insensitive to this parameter, since due to advection and diffusion processes in the disk and the existence of an outflow, the magnetic field profile is changed substantially over time. We therefore assume  $m = 0.5$  in general.

The relative strength of the magnetic field is governed by the magnetization parameter, generally defined as  $\mu_D = [B_p^2/2P]_{\theta=(\pi/2)}$ , the ratio between the poloidal magnetic field pressure and the thermal pressure. As it has been shown (Murphy et al. 2010; Sheikhezami et al. 2012; Stepanovs & Fendt 2014) the magnetic field distribution substantially changes over time. Therefore, the disk-jet dynamics is governed by the *actual* disk magnetization. The *initial* disk magnetization is denoted by  $\mu_0 = 0.5\epsilon/B_{p,0}$  and is calculated at the inner disk radius at the midplane and is set to be constant with radius. Typically, we apply  $\mu_0 \approx 0.01$ . We will further apply the notation  $\mu_D = \mu_D(R, t)$  for the time-dependent disk magnetization measured at the midplane. This will be the leading parameter of our paper.

As mentioned above, we obtain the initial disk density  $\rho_{\text{disk}}(R, \theta)$  and disk pressure  $P_{\text{disk}}(R, \theta)$  from integrating equation (6). As for  $\mu_D$ , the  $\rho_D(R)$  denotes the disk density along the midplane. Outside the disk the gas and pressure distribution is defined as hydrostatic “corona”,

$$\rho_{\text{cor}} = \rho_{\text{cor},0} R^{-1/(\gamma-1)}, \quad P_{\text{cor}} = \frac{\gamma-1}{\gamma} \rho_{\text{cor},0} R^{-\gamma/(\gamma-1)}, \quad (8)$$

where  $\rho_{\text{cor},0} = \delta \rho_{\text{disk}}(R=1, \theta=\pi/2)$  with  $\delta = 10^{-3}$  and the index 0 again referring to the initial value at the inner disk radius.

Although it is common to define an initial accretion velocity that balances the imposed diffusivity  $V_R = \eta J_\phi / B_\theta$ , we find that with our parameter setup this is not necessary (see paper I).

### 3.2. Boundary conditions

We apply the same boundary conditions as described in paper I. These are the standard symmetry conditions along the *rotational axis* and the *equatorial plane*. Along the radial boundaries of the domain, we distinguish two different areas. That is (i) a *disk boundary* for  $\theta > \frac{\pi}{2} - 2\epsilon^4$ , and (ii) a *coronal boundary* for  $\theta < \frac{\pi}{2} - 2\epsilon$ , and consider different conditions along them.

Along the *inner radial boundary* for all simulations we impose a constant slope for the poloidal component of the magnetic field. The magnetic field direction is axial near the axis,  $\theta = 0$ , while at the inner disk radius the inclination is  $70^\circ$  with respect to the disk surface. The method of constraint transport requires the definition of only the tangential component, thus to prescribe  $B_\theta$  along the innermost boundary. The normal component  $B_R$  follows from solving  $\nabla \cdot \mathbf{B} = 0$ . In order to implement the prescription of a constant magnetic field angle, we solve  $\nabla \cdot \mathbf{B} = 0$ , taking into account the ratio of the cell-centered magnetic field components  $B_\theta/B_R = -\tan(\varphi)$ . We start the integration from the axis ( $\theta = 0$ ), where

$B_\theta = 0$ . Thus, by fixing the slope of the magnetic lines, we allow the magnetic field strength to vary.

Along the *inner coronal boundary*, we prescribe a weak inflow into the domain with  $V_p = 0.2$ . This is meant to stabilize the inner coronal region between the rotational axis and the disk jet. By varying the slope of the magnetic field along this inner corona in the range of  $60 - 80$  degrees w.r.t. midplane, we found that it only slightly affects the slope of the innermost magnetic field lines. The global structure of the magnetic field is instead mainly governed by the diffusivity prescription. Since the inner boundary by design models the magnetic barrier of the star, we choose a rather steep slope in order to avoid the disk magnetic flux entering the coronal region.

Across the *inner disk boundary* (that is the accretion boundary) we extrapolate both the density and pressure by power laws,  $\rho R^{3/2} = \text{const}$ , and  $PR^{5/2} = \text{const}$ , respectively. Both the toroidal magnetic field as well as the toroidal velocity components are set to vanish at the inner coronal boundary,  $B_\phi = 0$ ,  $V_\phi = 0$ . For the inner disk boundary, we further apply the condition  $B_\phi \sim 1/r$  ( $J_\theta = 0$ ), and extrapolate the radial and the toroidal velocity by power laws,  $V_R R^{1/2} = \text{const}$ , and  $V_\phi R^{1/2} = \text{const}$ , respectively, while  $V_\theta = 0$ . For the inner disk boundary, only negative radial velocities are allowed, making the boundary to behave as a *sink*, that absorbs all material that is delivered by the accretion disk at the inner disk radius.

The *outer boundary conditions* have only little influence on the evolution of the jet launched from the very inner disk, as the application of spherical coordinates provides an opportunity to use a much larger simulation domain compared to cylindrical coordinates. We therefore extrapolate  $\rho$  and  $P$  with the initial power laws and apply the standard PLUTO outflow conditions for  $V_R, V_\theta, V_\phi$  at the outer boundary, thus zero gradient conditions. We further require  $B_\phi \sim 1/r$  ( $\vec{J}_\theta = 0$ ) for the toroidal magnetic field component, while a simple outflow condition is set for  $B_\theta^5$ . Again  $B_R$  is obtained from the  $\nabla \cdot \mathbf{B} = 0$ .

For the radial velocity component we distinguish between the coronal region, where we require positive velocities  $V_R \geq 0$ , and the disk region, where we enforce negative velocities  $V_R \leq 0$ .

### 3.3. The prescription for the magnetic diffusivity

The prescription for the magnetic diffusivity is essential for the evolution of the disk dynamics. Here we apply the same - so-called standard - prescription that is described in detail in paper I. In the following, we repeat some essentials from paper I.

#### 3.3.1. General approach

The magnetic diffusivity in accretion disks is considered to be of turbulent origin. Magnetized disks are subject to the magneto-rotational instability (MRI)

<sup>5</sup> Note that this condition may imply a Lorentz force that is confining along the outer boundary, as discussed by Ustyugova et al. (1999). This Lorentz force may affect the collimation and acceleration of the outflow. However, our outer boundary is at such a large distance that we consider these effects, if present, as marginal. In addition, a spherical grid minimizes this potential effect (Ustyugova et al. 1999).

<sup>4</sup> Note that  $2\epsilon \approx \arctan(2\epsilon)$



for moderate field strengths (Balbus & Hawley 1991; Fromang 2013), and to the Parker instability (Gressel 2010; Johansen & Levin 2008) for stronger disk magnetization. For strong fields the MRI modes become suppressed (Fromang 2013). On the other hand, a strong magnetic field may become buoyant, leading to the Parker instability. While the MRI is confined within the disk, the Parker instability operates closer to the surface of the disk where the toroidal magnetic field is stronger.

How the Parker instability operates in accretion disk is not quite obvious. Foglizzo & Tagger (1994) have found that under certain conditions a turn-over may happen that re-directs the up-lifted material back to the disk midplane.

A self-consistent study of the origin of the turbulence is beyond the scope of our paper. We therefore need specific prescription of the magnetic diffusivity. We apply an  $\alpha$ -prescription (Shakura & Sunyaev 1973) for the magnetic diffusivity, implicitly assuming that the diffusivity has a turbulent origin. In general the diffusivity distribution has three major parameters. That are the radial profile, the vertical profile, and the strength of diffusivity. The vertical profile may extend up to a level above the pressure scale height of the disk (see Gressel 2010; Sheikhezami et al. 2012; Fendt & Sheikhezami 2013). The radial profile is essential for the advection of disk material across the magnetic field penetrating the disk. Only for high magnetic diffusivity in the outer disk sufficient mass supply from the outer to the inner disk is possible, from where disk material is advected towards the central object or is ejected into the outflow (Stepanovs & Fendt 2014; Stepanovs et al. 2014)

### 3.3.2. Diffusivity description of the current paper

We have investigated a variety of diffusivity prescriptions, all of them can be represented in the following form for the poloidal magnetic diffusivity,

$$\eta_P = \alpha_{\text{ssm}}(\mu_D) C_s \cdot H \cdot F_\eta(z), \quad (9)$$

where the vertical profile of the diffusivity is described by a function

$$F_\eta(z) = \begin{cases} 1 & z \leq H \\ \exp(-2(\frac{z-H}{H})^2) & z > H, \end{cases}$$

that confines the diffusivity to the disk region (see paper I). The anisotropy parameter  $\chi \equiv \eta_T/\eta_P$  quantifies the different strength of poloidal and toroidal diffusivity. It is common to assume  $\chi$  of order of unity. For viscous disks Casse & Ferreira (2000) showed that there is a theoretical limit for  $\eta_T$ , namely  $\eta_T > \eta_P$ . Highly resolved disk simulations indeed suggest  $\chi \simeq 2 \dots 4$  (Lesur & Longaretti 2009), implying that the toroidal field component typically diffuses faster than the poloidal component.

Although a parameterization as in Eq. 9 is commonly used (except for a different profile function  $F_\eta(z)$  and the thermal scale height  $H_T$  instead of  $H$  as in our case), there are no clear constraints upon the value  $\alpha_{\text{ssm}}$  may take. Recent numerical modeling of the MRI applying a non-zero net magnetic field indicate rather high values,  $\alpha_{\text{ssm}} \simeq 0.08 - 1.0$ , with a corresponding magnetization  $10^{-4}, 10^{-2}$  (see Bai & Stone 2013 and our discussion in

paper I). Obviously, different functions of  $\alpha_{\text{ssm}}(\mu_D)$  will lead to a different disk evolution. We start from a general prescription for magnetic diffusivity applied by other authors before (Casse & Keppens 2004; Zanni et al. 2007; Sheikhezami et al. 2012),

$$\eta_P = \alpha_m V_A \cdot H \cdot F_\eta(z) \quad (10)$$

by applying  $\alpha_{\text{ssm}} = \alpha_m \sqrt{2\mu_D}$ , where  $V_A = B_P/\sqrt{\rho}$  is the Alfvén speed, and  $\mu_D$ ,  $C_s$ , and  $H$  are the magnetization, the adiabatic sound speed and the local disk height, respectively, measured at the disk midplane. We evolve  $\alpha_{\text{ssm}}$  and  $C_s$  in time, but for the sake of simplicity we keep  $H$  and  $F_\eta(z)$  constant in time, thus equal to the initial distribution.

The majority of simulations in the literature consider a magnetic field strength in equipartition with the gas pressure. Studying weakly magnetized disks, we have found that there exists an upper limit for the anisotropy parameter, above which the simulations show an irregular behavior (Stepanovs & Fendt 2014). In cases where the vertical velocity term can be neglected (e.g. for a very weak magnetic field with  $\mu_0 \leq 0.02$ ), the anisotropy parameter is  $\chi < 1/\alpha_m^2$ , which for our choice of  $\alpha_m$  is about 0.4. By probing the  $\chi$  parameter space we found that in order to obtain a stable accretion-outflow configuration for weakly magnetized disks, the  $\chi$  should be in the range 0.3 – 0.7. We therefore decided to apply  $\chi = 0.5$  for all of our simulations.

### 3.3.3. Comparison to literature works

The diffusivity profile we apply is constant in time and space (while its strength changes in time). We note that other authors have applied time-dependent diffusivity profiles so far, in particular adapting the strength and scale height of diffusivity following the time evolution of the isothermal sound speed and the Alfvén speed at the disk mid-plane. Such a consideration implies a strong feedback loop for the simulation that may give rise to an instable disk evaluation. This is why we have applied the simplified approach of a constant-in-time magnetic diffusivity profile.

In Murphy et al. (2010) the magnetic diffusivity is time-dependent and follows the turbulent viscosity that is updated considering the isothermal sound speed along the disk midplane (Prandtl number 2/3). The disk magnetization is not considered for the strength of the diffusivity. The vertical profile of the diffusivity is not discussed, and also not the numerical procedure how to practically update the scale height of the diffusivity distribution<sup>6</sup>

Tzeferacos et al. (2009) apply a magnetic diffusivity depending on the thermal scale height  $H$  and the Alfvén speed  $V_A$ , both calculated for the disk-midplane,  $\eta_m \propto H V_A \exp(-2z^2/H^2)$ . The authors do not further specify whether and how they update the magnetic diffusivity in

<sup>6</sup> It would be very interesting for the understanding of their simulations to see the time evolution of the diffusivity distribution (numerical values or maps). Further, the authors do not elaborate on their application of magnetic diffusivity on the scaled outer grid in their simulations. Because the user manual for PLUTO explicitly states that magnetic diffusivity should *not* be applied on stretched grids, the method implemented in Murphy et al. (2010) may be of use to the community at large.

time, the diffusivity distribution is described only as an initial condition.

In a previous publication (Sheikhnezhadi et al. 2012; Fendt & Sheikhnezhadi 2013) we have in particular investigated how the diffusivity profile affects jet launching and in particular mass loading. In Fendt & Sheikhnezhadi (2013) we have suggested a new time-dependent model for magnetic diffusivity that depends from the *local* disk pressure and magnetization. In particular the time evolution of the magnetic diffusivity has been shown.

On the other hand, the application of a diffusivity profile constant in time may have its caveats. That is that the disk may vertically shrink (quantified by the thermal disk height  $H_T(r, t)$ ), while the diffusivity remains vertically fixed with a fixed scale height for the diffusivity profile  $H$ . This may have a strong effect on the mass loading and, thus, on the jet dynamics.

A strong disk magnetic field may compress the disk hydrodynamic structure, however, this also depends on the field curvature and not only on the field strength.

Direct simulations of disk turbulence have shown that the disk turbulent diffusivity profile may indeed extend beyond the thermal scale height (Gressel 2010).

In summary, we believe that our choice of diffusivity indeed provides physically meaningful results. We see as an advantage of our diffusivity profile that we may control its functional form during the simulation at any time. We thus know its spatial distribution and may disentangle physical effects that depend on the local value for the diffusivity. Our diffusivity profile allow for a more stable simulation, as it allows for mass accretion and jet mass loading also when the disk thermal scale height becomes low.

From the simulations in the literature cited above, it becomes not clear, how the diffusivity profile actually looks like during the time evolution. In particular, when the thermal disk height becomes small, numerical diffusivity may affect the physical diffusivity such that the initially chosen functional form of diffusivity may actually not hold. We also believe that the grid resolution is usually not sufficient to allow for a physical treatment of the feedback between the disk midplane Alfvén velocity and the vertical profile of the disk turbulence that governs the magnetic diffusivity.

### 3.4. Simulation parameters

The magnetic diffusivity  $\eta = \alpha_m f(R, \Theta)$  consists of the magnetic diffusivity parameter  $\alpha_m$  that defines its strength and a function for the profile  $f(R, \Theta)$  (see above). The anisotropy parameter is chosen  $\chi = 0.5$ . In general the magnetic diffusivity also defines the trend for the disk magnetization - magnetic field amplification by advection versus magnetic field decline by diffusion<sup>7</sup>. The resulting magnetization - measured as a snapshot in time - determines the actual launching conditions.

The magnetic diffusivity parameter  $\alpha_m$  turns out to be crucial for obtaining a quasi-steady state solution. As discussed in paper I, there is a critical magnetic diffusiv-

<sup>7</sup> This balance can be denoted by the magnetic Reynolds number  $Re_M \equiv VL/\eta$  that relates dynamical and diffusive effects by comparing typical velocities  $V$  and length scales  $L$  to the diffusivity  $\eta$ .

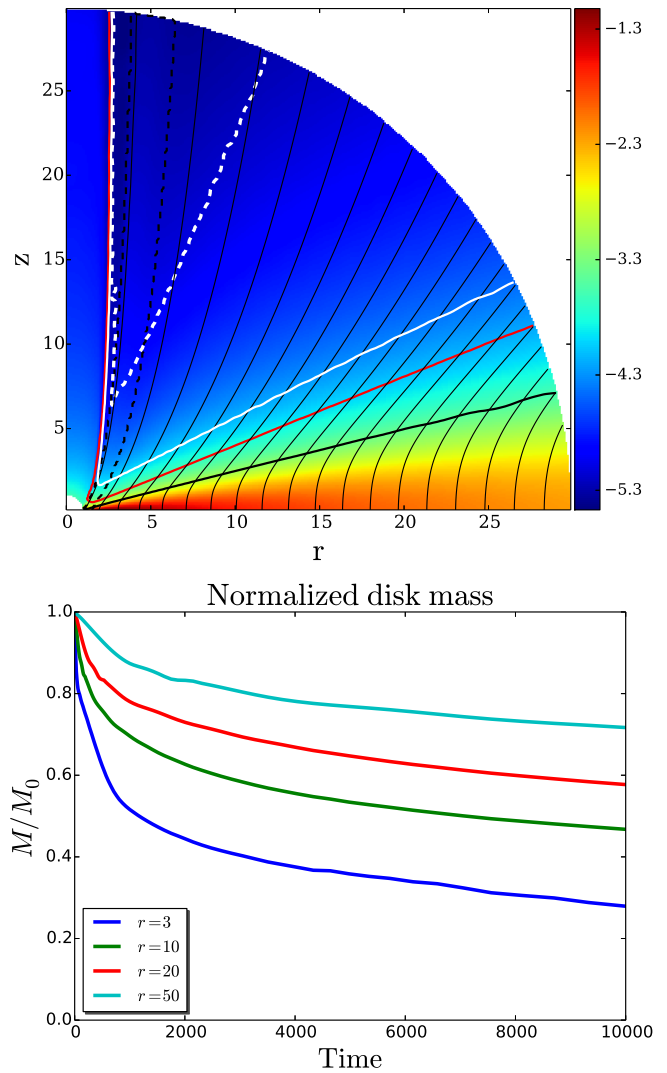


**Figure 1.** Typical structure of the disk-jet system at  $T = 10,000$  (top). Colors show logarithmic density. Thin black lines show the magnetic field lines. Thick dashed lines, rooted at  $r = 1.1$  and  $r = 1.5$ , mark the jet region, investigated further in the paper. Lines mark the disk surface (black), the sonic surface (red) the Alfvén surface (white), and the fast surface (dashed white). The jet sheet further investigated below is indicated by dashed black lines. The time evolution of the disk mass included within increasing radius decreases with time (below).

ity parameter  $\alpha_m$  such that for our standard diffusivity prescription the diffusive and advective processes are in balance.

For our setup, we find that  $\alpha_m \approx 1.6$  is a good choice for a smooth and long-term evolution of the simulation. However, a slight deviation from the critical value for the diffusivity parameter leads the simulation into a state that is dominated by either diffusion or advection. As the simulation progresses, this deviation amplifies (see paper I) and the actual quantities of the disk change. Essentially, this process allows us to investigate the disk-jet evolution over a wide range of the actual disk magnetization  $\mu = 2 \times 10^{-4} - 3 \times 10^{-0.5}$ , since the magnetic flux of the disk can be either advected inwards increasing the disk magnetization, or it can diffuse out leading to a lower disk magnetization.

When the actual disk magnetization is in the above

mentioned range, all simulations show a robust behavior over long time scales and can be smoothly evolved for more than 10,000 time units (corresponding to 1600 disk revolutions at the inner disk radius), until we stop the simulation. We are able, however, to perform simulations for more than 500,000 time steps (see paper I).

Table 1 summarizes all simulations discussed in this paper. We denote our simulations in alphabetical order according to the strength of the *initial* magnetization. The plus and minus signs indicate a slightly higher or lower diffusivity  $\alpha_m$  with respect to each other. We note, that a *lower* diffusivity parameter leads to *stronger* actual disk magnetization, as a result of faster advection and accumulation of the magnetic flux.

### 3.5. General jet-disk evolution

In paper I, we have presented an approach that allows us to study a broad parameter space of the disk-jet structure. While in paper I our discussion concentrated more on the disk evolution, in the present paper we are interested in the evolution of the outflow dynamics and how it correlates to the physical disk properties. In the following we briefly comment on the general evolution of the disk-outflow dynamics, mainly summarizing our simulations of paper I.

After starting the simulation from the initial conditions, the disk evolves into a new equilibrium. When the disk wind establishes, the efficient removal of angular momentum from the disk by the wind leads to accretion of disk material. A new dynamical state of the disk will be reached - defined by the balance between inward advection of mass and magnetic flux and outward diffusion of the magnetic flux.

The disk material is lifted vertically and couples to the magnetic field lines of jet and outflow.

The evolution of the accretion-ejection structure finally reaches a quasi steady state that is further affected by the mass loss due to accretion and ejection. Thus, the disk structure evolves slowly in time, while the outflow that is launched during quasi steady state, establishes on a much shorter time scale - that is the Keplerian time scale at the foot point of the outflow.

Figure 1 shows a small subset ( $z < 30$ ) of a large numerical grid of a typical simulation ( $z < 1500$ , see paper I). Here the structure of the disk-jet system has evolved until time  $T = 10,000$ . The location of typical surfaces, namely the disk surface, defined as the surface where the radial velocity changes sign,  $V_R = 0$ , the sonic surface and the fast magnetosonic surface, have become stationary, indicating that the disk-outflow structure in this volume has reached a quasi-steady state. We denote this evolutionary stage as a *quasi-steady* state, since there is still a very slow evolution of the system is for long time scales. This is because the inner part of the disk experiences a slow mass depletion by the accretion and ejection. Furthermore, it takes much longer for the outer part of the disk to evolve and thus to reach a steady state.

For the setup with the diffusivity parameter  $\alpha_m$  chosen about its critical value, it takes about 1000 dynamical time steps (thus 160 inner disk revolutions) to reach a quasi-steady state. The quasi-steady state situation is determined by the balance between accretion and ejection and also by the mass transfer rate from the disk to the jet.

The magnetic diffusivity acts to level out the magnetic field gradient, thus setting the overall structure of the magnetic field. However, one should keep in mind that the magnetic field strength and structure of real accretion disks are also not known. In our approach, we will compare the disk magnetization and the outflow characteristics that are both influenced by the magnetic diffusivity. As we will see, another diffusivity prescription will probably reach a different stage of disk magnetization at a different time, however, the jet characteristics we find from the simulation, are just dependent on the actual magnetization at the jet foot point. They are thus memoryless and do not depend on the “history” of how this state has been reached.

In order to correlate the jet dynamics to the underlying disk, we will apply the steady-state MHD conservation laws along the field lines. In general, these MHD integrals are conserved only in a steady-state, axisymmetric MHD. In our simulations we always reach a quasi-steady state for the high-speed jet component and the inner disk structure from where this jet is launched. In the case of a low disk magnetization ( $\mu_D \leq 0.001$ ), we find that the jet becomes slightly disturbed above the Alfvén surface. We believe that these perturbations are presumably triggered by the shear between the axial flow injected from the coronal boundary (as a boundary condition) and the jet that is physically launched from the inner disk. However, since the outflow remains in a quasi-steady state until it reaches the Alfvén surface, we may indeed consider the MHD integrals obtained at this location and interrelate them to the underlying disk magnetization. Therefore the correlations we obtain are valid also for the low magnetization case. In the case of a high disk magnetization, the outflow remains unperturbed and the MHD integrals remain conserved along the jet also for larger distances from the launching point.

Figure 1 (bottom) shows also the temporal evolution of the disk mass. We see that after a sharp initial decline, the disk mass is still decreasing slowly due to the mass loss by accretion into the inner boundary and ejection into the jet. For later evolutionary times the disk loses about 10% of its mass over 6000 dynamical time steps for e.g.  $r < 10$ , so the typical time scale when half of the disk mass is gone would be  $\tau_{\text{disk}} \simeq 30,000$  dynamical time steps. This time scale would be the time scale on which the disk evolution happens, as seen by the evolution of the disk magnetization<sup>8</sup>.

The disk diffusive time scale is much faster. For a typical magnetic diffusivity  $\eta \simeq 0.03$  the time scale for magnetic diffusion is  $\tau_\eta \equiv l^2/\eta \simeq 3,000$  if we consider the jet launching area  $l \simeq 10$ . Previous simulations have shown that a quasi steady-state between advection and diffusion of magnetic flux is reached (see discussion above and Sheikhnezami et al. 2012). This time scale is similar to the advection time scale  $\tau_{\text{adv}} \equiv l/v_{\text{acc}} \simeq 1,000$ , applying typical accretion velocities we measure in our simulation of  $v_{\text{acc}} \simeq 0.01$ .

The kinematic time scale for jet formation usually scales with the Keplerian time scale at the jet foot point -

<sup>8</sup> This is why we had to develop another magnetic diffusivity model for the very long-term evolution simulations (more than 500,000 dynamical time steps) in paper I, allowing for a sufficiently rapid mass replenishment from the outer disk to the inner disk.

**Table 1**

Parameter runs of our simulations, alphabetically labeled according to the initial disk magnetization at the inner disk radius  $\mu_0$ . The plus and minus sign indicate a slightly higher or lower diffusivity, respectively, denoted by the parameter  $\alpha_m$  (see Equation 10).

	A	B+	B	C+	C-	D+	D-	E+	E-	G	H
$\mu_0$	0.001	0.002	0.002	0.003	0.003	0.005	0.005	0.01	0.01	0.02	0.03
$\alpha_m$	1.6	1.6	1.5	1.65	1.6	1.6	1.55	1.65	1.6	1.8	1.65

**Table 2**

Comparison of typical times scales in the simulation runs. The exact values depend on the radius and may also somewhat change in time. Time unit is  $T_0 = R_0/V_{K,0}$ . In code units  $T_0 = 1.0$ . Shown are the jet kinematic or propagation time scale  $\tau_{\text{jet}}$ , the diffusive time scale  $\tau_\eta$ , the advection time scale  $\tau_{\text{adv}}$ , both considering a scale length of  $l = 10$  for the jet launching area, the disk “life time”  $\tau_{\text{disk}}$  during which the disk loses about 50% of its mass, and the time scale for the whole disk outflow to establish a dynamical steady state,  $\tau_{\text{outflow}}$ , that is the Keplerian time scale for the outer disk radii.

time scale	$\tau_{\text{jet}}$	$\tau_\eta$	$\tau_{\text{adv}}$	$\tau_{\text{disk}}$	$\tau_{\text{outflow}}$
time in $t_{\text{in}}$	160	3,000	1,000	30,000	$5 \times 10^6$

simply due to the fact the the jet typically reaches asymptotically the same velocity  $\tau_{\text{jet}} \simeq l_{\text{grid}}/v_{\text{jet}} = l_{\text{grid}}/v_{\text{Kep}}$ . Typically,  $\tau_{\text{jet}} \simeq 160$  for a grid size of 1000 inner disk radii and a jet launched from close to the inner disk radius. The overall structure of the outflow - in particular its collimation - depends, however, on the *overall* pressure and magnetic field distribution, and, thus, also on those parts of the outflow that are launched from the outer disk and that evolve on much larger Keplerian time scales. We may define a time scale considering the whole outflow structure  $\tau_{\text{outflow}} \simeq l_{\text{grid}}/v_{\text{Kep,grid}}$ . For the parameters used above we find  $\tau_{\text{outflow}} > 30,000 \tau_{\text{jet}}$ .

#### 4. CHARACTERISTIC OUTFLOW PROPERTIES

In paper I, we have explored the general structure and evolution of the simulations with emphasis mainly on the disk variables, namely accretion-ejection efficiency, and the corresponding fluxes of mass and energy. In this paper, our main concerns are the jet quantities, especially the jet integrals that can be compared to the steady-state MHD theory, and the strong correlation between the jet physical properties and the disk magnetization.

##### 4.1. Steady-state jet MHD integrals

Below we compare the dynamical parameters of the outflow in a quasi-steady state with the parameters of the classical steady-state MHD wind theory. In axisymmetric, stationary, ideal MHD there are four quantities that are conserved along the magnetic flux  $\Psi \equiv \int \vec{B}_p \cdot d\vec{A}$ , namely the mass loading per flux surface enclosing the magnetic flux  $\Psi$ ,

$$k(\Psi) = \frac{\rho V_p}{B_p}, \quad (11)$$

the angular velocity of the field lines

$$\Omega_F(\Psi) = \frac{V_\phi}{r} - \frac{k B_\phi}{\rho r}, \quad (12)$$

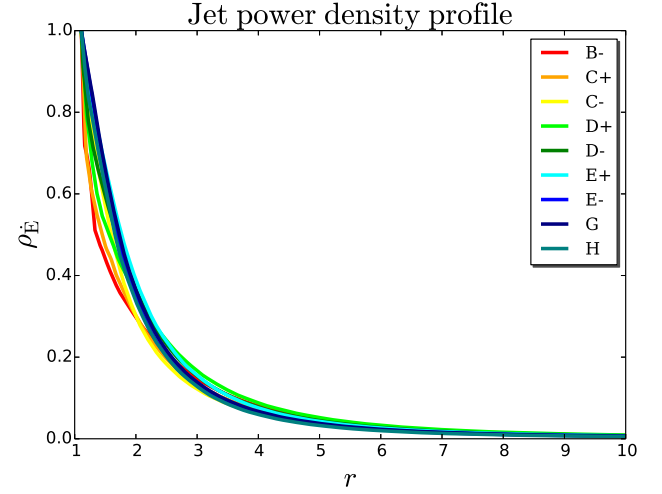


**Figure 2.** Profile of the jet power density  $\rho\dot{E}$  at  $T = 10,000$  along the surface  $z = H(r) + 1$  (parallel to the disk surface), normalized to the value at the inner edge of the surface at  $r = 1.1$ ,  $z = 1.22$ , for a range of parameter runs (see Table 1 for the notation).

the specific angular momentum

$$l(\Psi) = l_V + l_B = rV_\phi - \frac{rB_\phi}{k} \quad (13)$$

(with the kinematic and magnetic contributions  $l_V$  and  $l_B$ , respectively), and the specific energy

$$e(\Psi) = \frac{V_\phi^2 + V_p^2}{2} + \Phi_g + h + (l - rV_\phi)\Omega_F. \quad (14)$$

There are two more derived MHD integrals that are commonly used, namely

$$j(\Psi) = e - \Omega_F l, \quad (15)$$

that contains only kinematic quantities, and the maximum jet speed

$$V_{\text{inf}} = \sqrt{2e}, \quad (16)$$

that is the asymptotic speed of a propagating jet. For further details and derivations concerning the steady-state MHD jet integrals we refer to the review paper of Pudritz et al. (2007).

In order to explore the correlation of these integrals (calculated along the outflow) with the physical quantities describing the disk (mainly the actual disk magnetization), we normalize the integrals to their midplane values. In this paper, all jet integrals are presented in non-dimensional units, namely

$$\tilde{k} \equiv \frac{k}{\sqrt{\rho_D}}, \quad \tilde{w} \equiv \frac{\Omega_F}{\Omega_{F_D}}, \quad \tilde{l} \equiv \frac{l}{l_D}, \quad \tilde{e} \equiv \frac{e}{e_D}, \quad v_{\text{inf}} \equiv \sqrt{\tilde{e}}, \quad \tilde{j} \equiv \frac{j}{j_D}, \quad (17)$$



where the index “D” denotes the value calculated at the disk midplane (at a certain radius). In the following we will omit the tilde sign for simplicity<sup>9</sup>. Note that the underlying disk remains (sub-) Keplerian at the midplane during all simulations, thus  $V_\phi \propto r^{-0.5}$ . Therefore, the  $\Omega_{F,0}, l_D, e_D, j_D$  are constants in time, but the density  $\rho_D$  varies as disk evolves. For example,  $l = 3$  corresponds to the jet layer whose *specific* angular momentum is three times higher than the specific angular momentum of the underlying Keplerian disk at the jet layer foot point (at the midplane).

#### 4.2. How to quantify the disk and jet properties

The jet integrals are essential outflow properties that potentially connect the asymptotic outflow to the disk properties. Naturally, the numerical results are calculated on numerical grid points. Thus, some averaging procedure is required to derive the jet integrals along a magnetic flux surface that is intersecting the grid cells. Here, we briefly describe how we calculate the integrals from the numerical simulation. Such a prescription has not always been provided in the literature.

We obtain the number value for each jet integral by averaging across an outflow sheet of certain width and length located just beyond at the Alfvén surface. This average is performed as a snapshot for a certain time. For each of the integrals we have explicitly checked whether it is conserved along the corresponding sheet along the outflow.

The extent of the averaging area should be at one hand narrow enough in order to provide a meaningful value for the flux surface. On the other hand it must be large enough to provide an accurate average value. We consider a jet sheet that is confined between two “adjacent” magnetic flux surfaces and that is rooted in the innermost disk between  $r = 1.1$  and  $r = 1.5$ . From here the most powerful part of the jet is launched. The radius  $r = 1.1$  is well separated from the inner boundary by eight grid cells.

For the length of the averaging domain, we take a “box” ranging from the Alfvén point of that flux surface  $z_A$  to  $(z_A + 2.0)$ . Depending on the vertical position along the flux surfaces, the radial separation between the flux surfaces varies (it is  $\Delta r = 0.4$  only at the equatorial plane).

We will refer to  $X_D = X(0)$  as the disk quantities (at the foot point of the jet), while  $X_A = X(z_A)$  denote the jet quantities. By computing average values over a bundle of magnetic flux surfaces (a jet sheet) we are able to provide a robust measure for the integrals.

This can be demonstrated by e.g. exploring the radial profile of different physical quantities along the disk surface - thus by comparing the properties of different sheets of the jet. As an example, Figure 2 shows the radial profiles of the jet power density  $\rho_e = \rho e V_\phi$  along a surface  $z = H(r) + 1$  parallel to the disk surface<sup>10</sup>. These profiles were all plotted at the same time,  $T = 10,000$ .

<sup>9</sup> Note that we apply the notation Pudritz et al. (2007) and (Pelletier & Pudritz 1992). This differs somewhat from the notation used e.g. in Blandford & Payne (1982) or Casse & Ferreira (2000), who denote the mass loading per flux surface with  $\kappa$  and the specific angular momentum with  $\lambda$ .

<sup>10</sup> Note that all different the lines correspond to different simulation runs

We find that all profiles follow a very similar shape, thereby approving our average measure for the jet parameters along the inner most jet sheet as indeed representative for the jet as a whole. Note that the underlying disk properties are completely different as resulting from different simulations which started from different initial conditions and evolve differently. In particular, the actual magnetization, the density distribution or the accretion velocity are different for each of the simulations.

#### 4.3. Conserved quantities along the jet

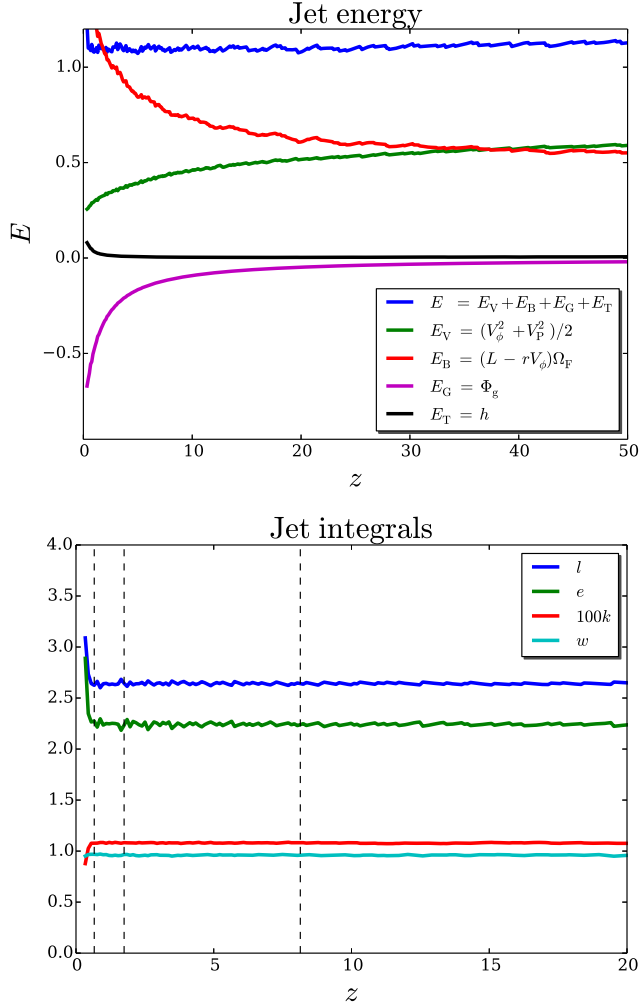
In this section, we discuss how the physical jet properties vary along the outflow. We follow the outflow from its foot point to the asymptotic domain. Note that when referring to the z-axis in following figures, all quantities are averaged over the jet layer, although the plot is along the z-axis.

Figure 3 (top) shows the profiles along the jet for the different jet specific energy components for simulation run *B*. We see that although we have averaged the variables within a jet layer containing a bunch of magnetic field lines, the total energy  $e = e(\Psi(r, z))$  is well conserved along the jet, approving our averaging approach. The same is true for all jet integrals studied in this paper. The thermal energy is negligible everywhere in the jet. The gravitational energy is negligible only far from the disk ( $Z > 20$ ). Here the outflow velocity has surpassed the local escape speed  $V_P(R, \theta) \gg V_{\text{escape}}(R, \theta)$  and has become gravitationally unbound to the central object. Figure 3 (top) further indicates how the magnetic energy of the jet is transferred into the jet kinetic energy. Far from the disk the transformation of the magnetic energy into the kinetic energy becomes less efficient. This decrease of acceleration is related to the increase of collimation.

Figure 3 (bottom) shows the profiles along the jet for the other MHD integrals. Shown are the jet angular momentum  $l$ , the mass load (multiplied by a factor 100), the field line angular velocity  $\omega$ , and the jet energy  $e$ . Vertical lines indicate the position of the magnetosonic surfaces. The sonic surface and the slow magnetosonic surface are indistinguishable. the Alfvén surface, and the fast magnetosonic surface, respectively. The bottom figure demonstrates that our approach for averaging discussed above is working fine, as all integrals follow a straight line already at the Alfvén surface.

Figure 4 indicates how efficient the magnetic angular momentum is transferred into kinetic angular momentum. We show the angular momentum balance along the jet for two different evolutionary times. We see that the rate of the angular momentum transfer along the jet is different for different evolutionary times. At earlier times ( $T = 1,000$ ) the magnetic angular momentum is transferred faster into the kinetic angular momentum compared to later times ( $T = 10,000$ ). However, what is actually happening is that between these time steps the underlying disk magnetization has substantially changed from  $\mu_D \approx 0.02$  at  $T = 1,000$  to  $\mu_D \approx 0.2$  at  $T = 10,000$ .

From our simulations we may therefore conclude that for jets launched from a stronger magnetized disk it takes more time to convert all magnetic energy into jet kinetic energy. Further investigations are needed to clarify this point.



**Figure 3.** Jet specific energy contributions along the vertical direction  $z$  for the simulation  $B$  simulation at time  $T = 10,000$  (top). Different energy components are indicated by colors: total (blue), kinetic (green), magnetic (red), gravitational (magenta), and thermal (black) energy. Jet integrals along the magnetic field line rooted in the innermost disk are for simulation  $E+$  time  $T = 10,000$  (bottom). Shown are the jet specific angular momentum  $l$ , the mass load (multiplied by a factor 100), the field line angular velocity  $\omega$ , and the jet specific energy  $e$  (normalized as described in Eq. 17). Vertical lines indicate the position of the sonic surface / slow magnetosonic surface (indistinguishable), the Alfvén surface, and the fast magnetosonic surface, respectively.

## 5. THE DISK - JET CONNECTION

In this section, we obtain a number of correlations between the jet physical properties and the properties of the accretion disk. Our main motivation is the question *what kind of disks drive what kind of jets?*

As discussed in Section 4.2, the properties of the accretion disk can be specified by a few parameters that are quantified at the midplane of the inner disk. On the other hand, the parameters of the jet can be specified by the MHD integrals that are calculated by averaging across the inner jet layer at the location of the Alfvén surface (thus in the ideal MHD region of the outflow).

The material along the midplane is accreted through the inner boundary and is not ejected into the jet. However, the disk-jet system is tightly connected and the dynamics of both components follow a common global

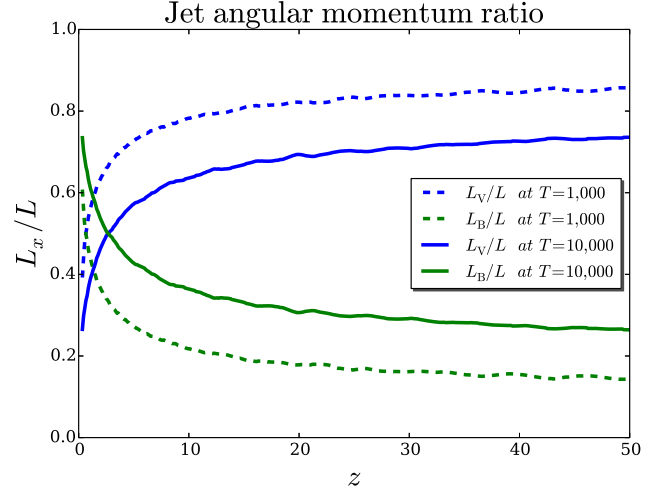


**Figure 4.** Jet angular momentum components along the jet, obtained for the  $B$  simulation. Kinetic (blue lines) and magnetic (green lines) to total jet angular momentum ratios are plotted at  $T = 1000$  (dashed lines) and  $T = 10,000$  (solid lines).

pattern. Even though the inner disk midplane and the outflow at the Alfvén point are not directly connected by the exchange of material itself, they are in causal connection due to magnetohydrodynamic waves and forces. The evolution of disk and outflow is interrelated and cannot be separately treated. It is therefore not surprising that all jet integrals discussed in the Section 4.1 can be, as we will see later, obtained by knowing the disk magnetization.

Figure 5 shows the correlations between the disk magnetization and the jet kinematic properties, the total (specific) jet angular momentum, the specific jet specific energy, and the mass load parameter, all measured at the Alfvén surface. Each of the short lines shown in the plots is the result of a long-term evolution of a certain simulation (labeled with A, ..., H). Each simulation has started from a different initial disk magnetization and has followed a different time evolution.

One way to correlate the jet kinematic properties to the underlying Keplerian disk properties is to assume that the energy and angular momentum at the disk surface are predominantly of kinematic origin (Anderson et al. 2003). As a consequence, the  $j$  and  $\omega$  integrals (see Equations 15 and 12) do *not* depend on the underlying disk properties. In other words, the relation between the jet energy and jet angular momentum is linear, see the definition Equation (15).

This is not true anymore if the underlying disk is strongly magnetized. Figure 5 (upper left) shows the jet angular velocity  $\omega$  with respect the disk magnetization. As we can clearly see, this physical variable now strongly depends on the disk magnetization (this is also true for the kinematic integral  $j$ ). Although both, the angular velocity  $\omega$  and the kinematic integral  $j$  of the jet are not constant, there is still a tight relation between the jet energy and the jet angular momentum (Figure 6). This relation is almost linear, but seem to follow two different linear regimes with a break at about  $l \simeq 2.7$ . It is interesting to compare this curve to the theoretical result for cold jets  $e = l - 3/2$  (Pelletier & Pudritz 1992; Pudritz et al. 2007) that would correspond to a straight

line below our numerically obtained relation shown in Figure 6). Thus, the jets launched in our simulations have more energy than theoretically expected for cold jets. This seems plausible as we do not consider cold jets but jets which carry some amount of enthalpy  $h$  (in normalized units). Therefore, a relation

$$e = l - 3/2 + h \quad (18)$$

is expected between specific energy and specific angular momentum. For  $l \lesssim 2.7$  our curve follows a relation with  $h \simeq e/2$ , thus with a larger slope, while for  $l \gtrsim 2.7$  our curve follows a relation with  $h \simeq 4/3$ , resulting in a slope similar to cold jets, but offset by the enthalpy  $h = 4/3$ .

Figure 5 (upper right) shows the correlation between the actual disk magnetization and the total jet angular momentum. Since the actual disk magnetization changes with evolutionary time, the corresponding jet angular momentum changes as well. It can be noted that all simulations follow the same general trend - no matter at what evolutionary stage the actual simulation is. A clear correlation between the disk magnetization and the jet angular momentum is established - the higher the disk magnetization the more angular momentum is extracted by the outflow.

Similarly, Figure 5 (lower left) shows the correlation between the jet energy  $e$  and the disk magnetization  $\mu_D$ . We note that the magnetization is plotted logarithmically, while the energy is plotted in linear scale. The curve shows a tight relation between the jet energy and the underlying disk magnetization - the stronger the disk magnetization  $\mu_D$  the higher the jet energy  $e$ .

We confirm the existence of the critical magnetization  $\mu_{\text{crit}} \approx 0.01\text{--}0.05$  found in paper I, where the ejection-accretion process was examined. Considering the change in the slope in Figure 5 (lower left), also the correlation between the jet energy and the disk magnetization indicates two different regimes, separated at  $\mu_{\text{crit}}$ . As we have shown in paper I, below the critical magnetization the toroidal magnetic pressure gradient plays a leading role in the outflow launching. The jets launched from this kind of configurations are usually known as “magnetic tower jets”. For a magnetization above the critical value, the magneto-centrifugal acceleration is dominating. The existence of these two regimes has been discussed by Ferreira (1997) considering the outflow ejection efficiency indices. Low ejection efficiencies should lead to powerful centrifugally driven jets, high efficiencies to magnetic pressure-driven jets. Here, we find a similar dichotomy, now in the framework of the disk magnetization.

The mass loading parameter  $k$  (see Equations 11 and 17) measures the amount of the matter that is ejected per unit magnetic flux. Figure 5 (lower right) shows the correlation between the mass loading parameter  $k$  and the disk midplane magnetization. We see that for this MHD integral the different simulations converge not as tightly as for the integrals discussed before.

This is a result of the *gas density* present in the definition of  $k$  (see Equation 17). Since the curves plotted in the figures show the continuous evolution of the disk-jet system, the disk and outflow densities are in principle different - within each simulation and even more between different simulations. Considering these circumstances, the correlation shown in Figure 9 (bottom) is *remark-*

*ably* tight.

As pointed out by Ferreira (1997), since cold jets can carry away the whole disk angular momentum, we may expect to find a systematic relation between mass loading and lever arm. In fact, from our simulations we can confirm the existence of such a relation - an even stronger relation than it was previously thought (Ferreira 1997; Ouyed & Pudritz 1997). We find that for a disk magnetization lower than critical,  $\mu_D < \mu_{\text{crit}}$ , the Alfvén lever arm follows a steep power law,  $\lambda \propto k^{-5.8}$ , while for  $\mu_D > \mu_{\text{crit}}$  the power law is flatter,  $\lambda \propto k^{-2.3}$ . These relations simply follow from combining the correlation between  $\lambda$  and  $\mu_D$  in Figure 5 with that combining  $k$  and  $\mu_D$ .

Another useful quantity is the Alfvén lever arm,  $\lambda = r_A/r_0$  (not shown). It can be shown that it directly links the mass ejection and accretion rates (Pelletier & Pudritz 1992),  $\dot{M}_{\text{acc}} \sim \lambda^2 \dot{M}_{\text{ej}}$ <sup>11</sup>. The jet angular momentum is related to the jet angular velocity through the Alfvén lever arm  $l = \lambda^2 \omega$ . In Figure 5 (bottom) we show a relation between the square of the lever arm  $\lambda^2$  and the disk magnetization  $\mu_D$ . As for the jet energy and angular momentum, we see a strong relation of the Alfvén lever arm with respect to the disk magnetization. For a higher disk magnetization, the length of the Alfvén lever arm increases. In case of a large Alfvén lever arm, more angular momentum is extracted from the disk. Along with the angular momentum, also energy is extracted more efficiently. These jets, carrying more angular momentum and energy, eventually become faster and wider. Essentially, this is the regime of the Blandford-Payne magneto-centrifugal acceleration.

The clear correlations we found in our simulations provides a potential tool for understanding of the launching conditions of observed jets. Knowing the jet energy  $e$  would immediately provide us with the information of the actual magnetization in the disk that launches this outflow. We note, that jet energy  $e$  is a dimensionless quantity that incorporates the knowledge both of the jet and its foot point (see Equation 17).

The steady-state MHD conservation laws allow us, in principle, to connect the observed jet quantities far from the source to the launching conditions. Blandford & Payne (1982) already provided analytical expressions for the energy and angular momentum partition for self-similar cold jets. Far from the source they find a ratio of Poynting flux to kinetic energy flux of  $2/(M_{\text{FM}}^2 - 2)$  for outflows with a fast magnetosonic Mach number  $M_{\text{FM}} > 1$ . Applied to protostellar jets with typically  $M_{\text{FM}} \simeq 3$ , this corresponds to jets that are kinematically dominated by a factor four.

Essentially, the jet terminal speed - defined by the jet terminal kinetic energy/momentum - depends on how much of the *magnetic* energy/momentum is left in comparison to the kinetic parts. When the jet leaves the disk and enters the ideal MHD regime, the specific energy and specific angular momentum become fixed. As the jet propagates, the magnetic energy and magnetic angular momentum are transferred into kinetic energy and

<sup>11</sup> Note that this is a simplistic approximation for our case and holds only for one field line. In general, both  $\dot{M}_{\text{acc}}$  and  $\dot{M}_{\text{ej}}$  both depend on radius - as the accretion rate lowers when accreted matter becomes ejected from the disk.

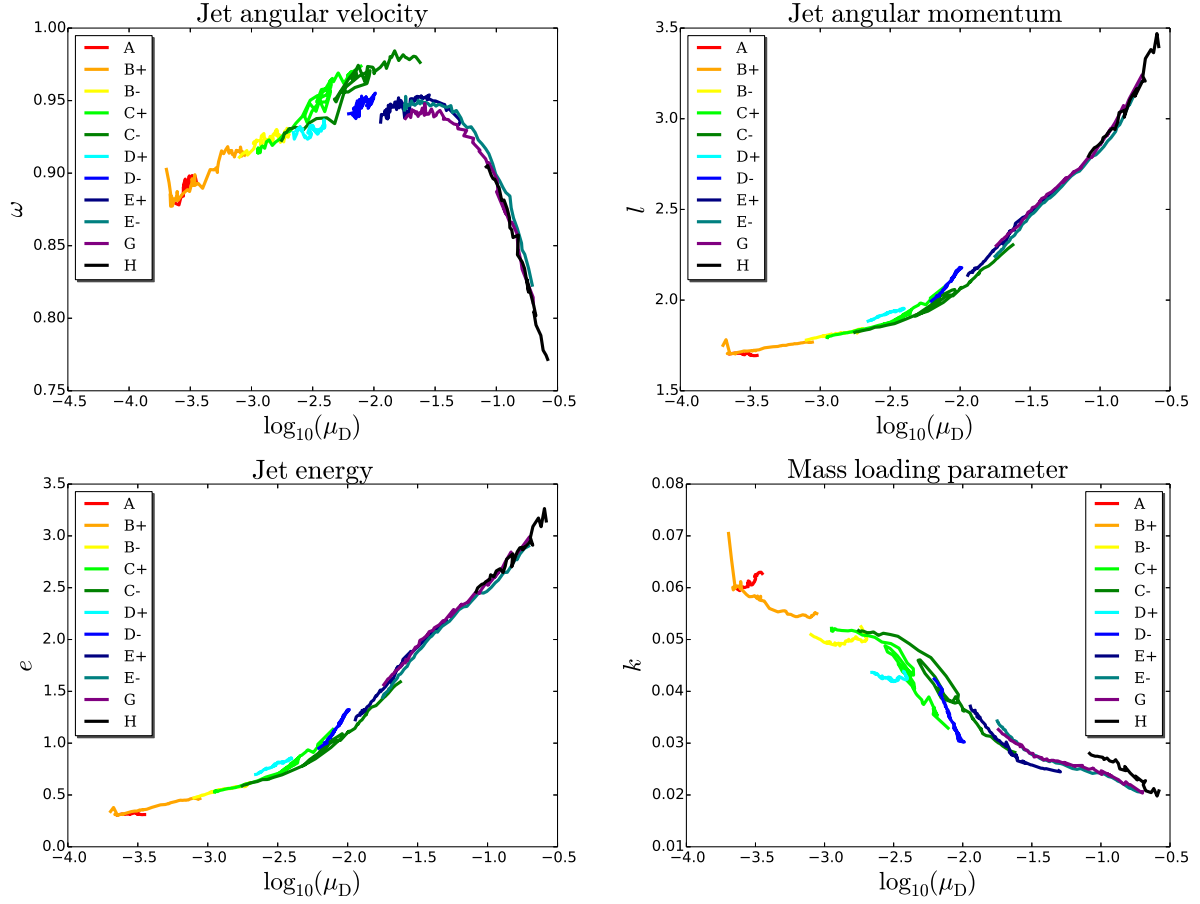


**Figure 5.** Jet physical properties with respect to the disk magnetization  $\mu_D$ . Shown is the jet angular velocity  $\omega$ , the specific angular momentum  $l$ , the jet energy  $e$ , and mass loading parameter  $k$ . Each line represents the evolution of a single simulation (see Table 1) from 700 to 10,000 time units.

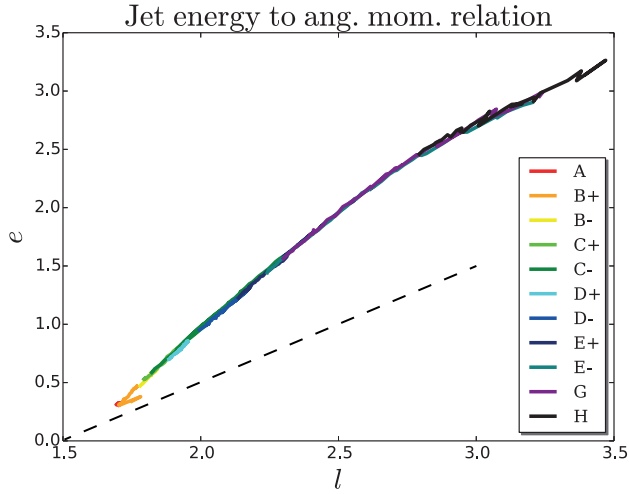


**Figure 6.** Jet specific energy  $e$  with respect to the jet specific angular momentum  $l$ . Each line represents the evolution of single a simulation (see Table 1) from 700 to 10,000 time units. The dashed line indicates the theoretical relation for cold jets  $e = l - 3/2$ .

kinetic angular momentum. However, our simulation domain does not yet reach the asymptotic regime where energy and angular momentum conversion has converged.

In Figure 7, we show the maximum poloidal speed of the jet,  $v_{\max} = \max_z(V_P)$ , as defined by Equation 16, with respect to the theoretical limit for the jet velocity.

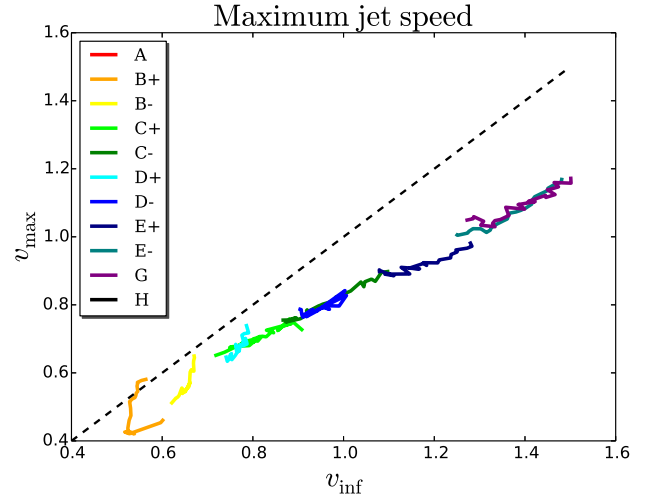


**Figure 7.** Jet maximum speed  $v_{\max}$  as measured in the domain with respect to the maximal jet speed estimated from the jet energy  $e$ . Each line represents the evolution of a single simulation (see Table 1) from 3,000 to 10,000 time units.

ity. The velocity  $v_{\max}$  is measured as the maximum speed of the jet in the whole domain as soon as a quasi steady state of the simulation has been reached. We find that in our simulations the theoretical limit is never reached. The maximum speed obtained within the domain is about 75% of the theoretical limit.



There may be several reasons for this. First, the high-velocity jets obtained in simulations show a high degree of collimation. This is different to e.g. self-similar studies, or studies that assume a parabolic field distribution in general, both implicitly assuming that the magnetic flux diverges at infinity. Therefore, some of the magnetic field energy is conserved along the flow as well as some gas enthalpy, and not all energy is transformed into kinetic energy of the jet.

Another reason may be that energy conversion from magnetic to kinetic energy may indeed take longer as the domain size allows. Yet another reason may be the lack of resolution across the jet for very long distance in propagation direction (typical for a cylindrical jet on a spherical grid) - indeed we found that an increase/decrease of the resolution across the jet leads to a higher/lower jet maximum speed obtained in the domain. While we can resolve the disk and the launching area with rather good resolution, the area of the collimated jet becomes less and less resolved along the direction of jet propagation. We suspect that this may lower the efficiency of energy conversion from magnetic to kinetic energy and also that the energy that is carried along the jet is somewhat lost, “diffused” away from the central spine.

## 6. THE ACCRETION-EJECTION PROCESS

In order to compute the mass, energy, and angular momentum fluxes, we need to consider the correlations between the densities and velocities for both accretion and ejection.

### 6.1. Mass loading and Alfvén lever arm

It is helpful to introduce the mass stream ratio  $\zeta$  that compares the properties of the ejected gas (i.e. the stream of the mass along the magnetic flux surface) at the Alfvén point to the value measured at the disk mid-plane,

$$\zeta = \frac{\rho_A V_{P,A}}{\rho_D V_{P,D}}. \quad (19)$$

Here,  $\rho$  is the density and  $V_P$  the poloidal velocity at the disk midplane (subscript D) and Alfvén point (subscript A), respectively. Note, that  $V_{P,D} = V_R$ , as the only poloidal component at the disk midplane is radial. In Figure 9 (top) we show the mass stream ratio with respect to the disk magnetization. We find a clear and very tight correlation between these quantities. We note that this is a log-log plot indicating that the mass stream ratio is much smaller for the case of strong disk magnetization. In the case of weak and moderately strong magnetization,  $\mu_D < 0.1$ , we find a relation  $\zeta \propto \log(\mu_D)$  (not shown), thus a weak dependence of  $\zeta$  from the disk magnetization.

It is known that there is also a tight correlation between the disk magnetization and the mean accretion Mach number  $M_R = V_{P,D}/C_s$  (see e.g. Ferreira & Pelletier 1995; Königl & Salmeron 2011, or paper I). Figure 9 (middle) presents this relation for a wide range of the disk magnetization. Our simulations confirm a tight relation between the mean accretion Mach number and the disk magnetization - also for the case of weakly magnetized disk. The fact that the slope of the curves shown in Figure 9 (middle) changes, indicates that the accretion Mach number may grow at

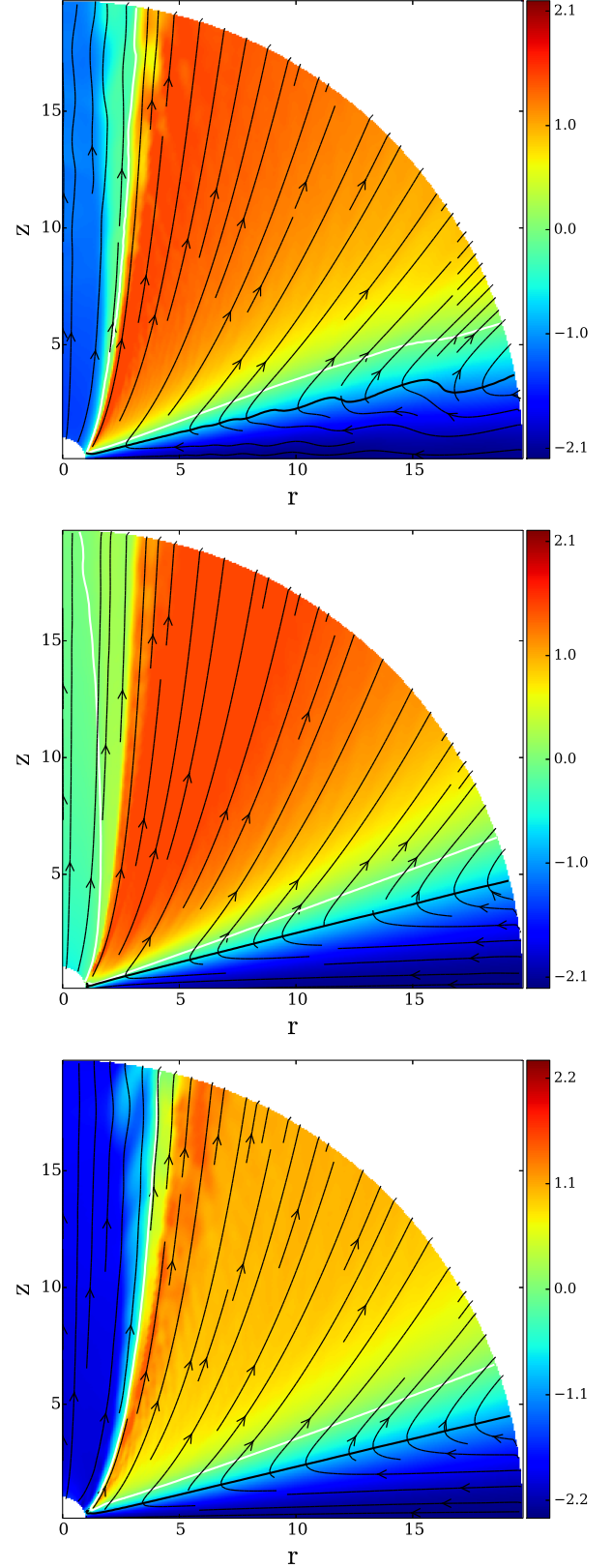


**Figure 8.** Disk-jet magnetization  $\mu(r, \theta)$  for simulation E+ at  $t = 1000$  (top) and  $t = 10000$  (middle), and for simulation D+ at  $t = 10000$  (bottom). Shown is the 2D magnetization distribution  $\log(\mu(r, \theta))$  (color coded), the surface where  $\mu = 1.0$  (white line), the stream lines (thin lines with arrows), and the launching surface where  $v_r = 0$  (black line).

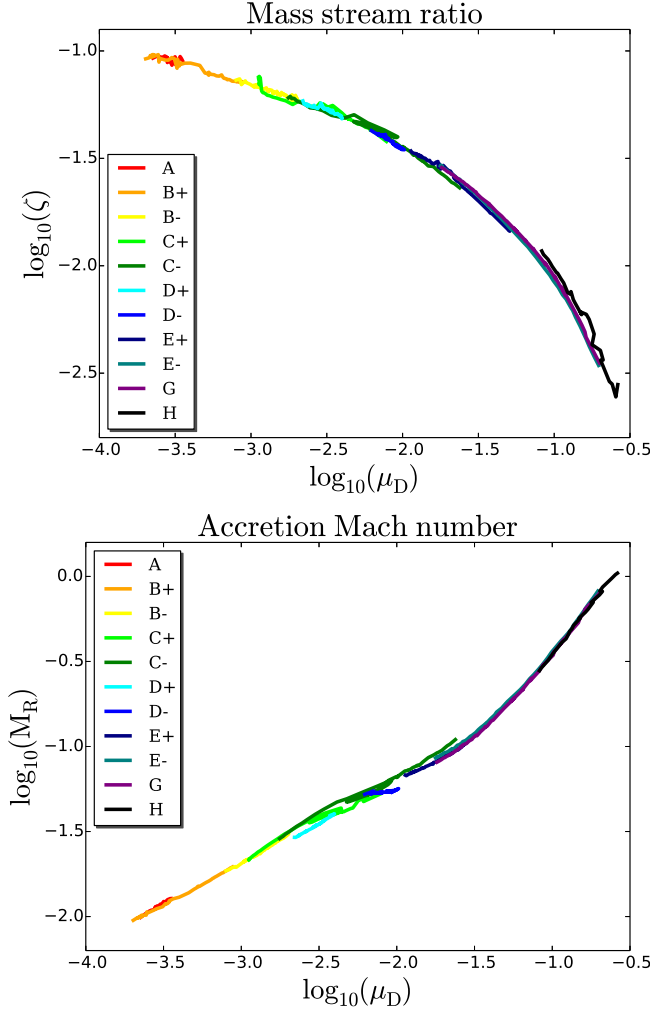


**Figure 9.** Accretion-ejection properties with respect to the disk magnetization  $\mu_D$ . Shown is the mass stream ratio  $\zeta$  (top) and the accretion Mach number (bottom). Each line represents the evolution of a single simulation (see Table 1) from 700 to 10,000 time units.

different rates when the the disk magnetization increases. We again emphasize that the physical quantities plotted in Figure 9 (middle) do not belong to the same mass flow within one particular simulation, but they are obtained from different simulations. Therefore, the relation we find is very general. It is a consequence of the fact that the ejection and accretion processes are tightly connected.

Figure 10 shows the mass loading parameter  $k$  with respect to the jet angular momentum  $l$ . This presentation is similar to the classic diagram presented in Blandford & Payne (1982) and Casse & Ferreira (2000) who plot the correlation between lever arm and mass loading<sup>12</sup>. We have plotted  $k(l)$  and not  $k(\lambda)$ , however, since  $l = \lambda^2 \omega$ , and  $\omega \simeq 0.9$ , the presentations are directly comparable to the literature cited above. Note that these figures shows the correlation between two jet properties - an correlation as already expected from the steady MHD theory while Figure 9 (bottom) essentially

<sup>12</sup> Note our slightly different notation. Our definition of  $\lambda^2$  corresponds to their  $\lambda \equiv (r_A/r_0)^2$  (Casse & Ferreira 2000), while our  $k$  is similar to their  $\kappa$ .

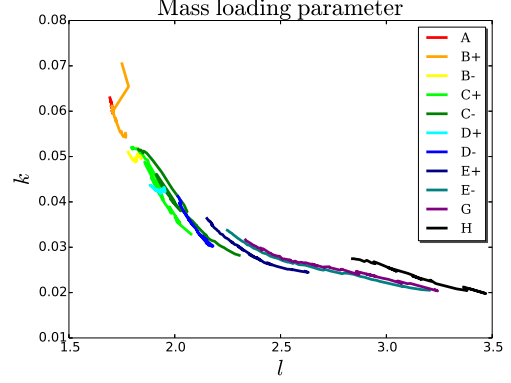


**Figure 10.** Mass loading parameter  $k$  and specific angular momentum  $l$ . Each line represents the evolution of a single simulation (see Table 1) from 700 to 10,000 time units.

correlates jet properties to the underlying disk properties. We first note that our curves follow the same trend as for the literature papers - an increase in  $k$  by a factor of 3 implies an decrease in  $l \simeq \lambda^2$  by a factor 2 in our case, while for Casse & Ferreira (2000) we find an increase in their  $\kappa$  by a factor of 4 with a corresponding decrease in  $\lambda$  (our  $\lambda^2$ ) by a factor 2 (for their  $\omega_A = 1.3$ ).

We interpret this as a general agreement concerning the *physics* of the mass loading process. However, there is a strong difference in the number values for the lever arm. While in our case  $l \simeq \lambda^2 \simeq 2...3$ , Blandford & Payne (1982) and Casse & Ferreira (2000) find lever arms of typically 7...10. We interpret this difference as a difference of the *geometry* of the accretion-ejection structure. In general, the lever arm found in our simulations are smaller than those derived from analytic models. In the simulations, the outflow ejected from the inner disk seem to either become collimated so fast that the Alfvén point along the magnetic field line is not far in radius from the foot point of the field line, or the Alfvén surface is located close to the launching surface of the flow that has not yet expanded when it becomes Alfvénic. An example of the latter can be seen in Murphy et al. (2010) (Fig. 1). To our knowledge this is a general behavior found in simulations of jet formation (independent whether they include disk structure or not in their simulations). Whether this effect is due to a principle difference in the geometry of the system, and maybe related to the self-similar approach of the steady-state solutions, is an essential question of jet launching and needs to be addressed in a future study.

In order to disentangle the different mechanisms affecting the ejection process, we rewrite the mass loading parameter  $k$  using the quantities introduced and discussed above,

$$k = \frac{\sqrt{\gamma} M_R \zeta \lambda^2}{\sqrt{2\mu}}, \quad (20)$$

where we applied  $B_{P,A} = B_{P,D}/\lambda^2$ . This equation simply follows from substituting  $M_R = V_{P,D}/C_s$  and  $B_{P,D}/\sqrt{\rho_D} = \sqrt{2\mu} C_s^T$  into Equation 11 and 17.

We can now compare how the different variables in the mass loading parameter change with the disk magnetization, and, thus affect  $k$ . As we have previously discussed, in the case of the moderately magnetized disk, the accretion Mach number increases almost linearly with the disk magnetization (see above and paper I). From Fig-

ure 5 (lower right) it becomes obvious that the Alfvén lever arm squared  $\lambda^2$  also increases with the disk magnetization. However, this increase is rather weak - a change in the disk magnetization by three orders of magnitude leads only to a factor two in the change of  $\lambda^2$ . We have, however, found above that the mass loading parameter  $k$ , *decreases* with the disk magnetization. One possible explanation for this behavior is that the ejection to accretion stream ratio,  $\zeta$ , decreases very quickly with the magnetization, as we have shown in Figure 9 (top). Note that analytical models are able to provide an exact link between the lever arm  $\lambda$ , the mass load parameter  $k$ , and a parameter that quantifies the so-called ejection efficiency  $\xi$  (Ferreira 1997; Casse & Ferreira 2000).

### 6.2. Jet launching and acceleration

In this section, we finally discuss the difference in the jet-launching mechanism for different disk magnetizations. In paper I we have found indication for a critical value for the disk magnetization  $\mu_{\text{crit}} \approx 0.03$  that seem to separate two regimes of disk dynamics. These two regimes can be referred to as advection or diffusion dominated, respectively.

Here, we would like to confirm this finding again by considering the magnetic Reynolds number for accretion  $Re_m = V_R H / \eta$ , where  $V_R = 4\mu_D C_s$  approximates the accretion velocity and  $\eta = \alpha_m \sqrt{\mu_D} C_s H$  corresponds to the magnetic diffusivity prescription applied. Thus, the resulting accretion Reynolds number depends mainly on the disk magnetization  $\mu$  and the diffusivity parameter  $\alpha_m$

$$Re_m \approx 2\sqrt{2} \frac{\mu_D}{\alpha_m}. \quad (21)$$

However, this is an approximation and serves mainly to illustrate the accretion-diffusion balance. We found that the diffusivity parameter  $\alpha_m \sim 1.6$  yields a quasi-steady state regime for accretion such that diffusion and advection are roughly in balance (thus  $Re_m \sim 1$ ). In other words, the same amount of the magnetic flux carried inward by the accretion is diffused outward. We note that the aforementioned reasoning can be only qualitative, as the physical evolution of the system is highly complex.

By examining the properties of the jets launched from the disks, we can distinguish two different, but complementary regimes of the jet launching. This can be seen, for example, in Figure 5 (upper left), where we find a prominent peak in the jet angular velocity around  $\mu_D \approx 0.01 - 0.05$ . In order to better understand what is the difference between these regimes, we now present several jet quantities computed at the Alfvén point.

Figure 11 shows the ratio of toroidal to poloidal velocity (top) and magnetic field (bottom), computed at the Alfvén point. As the disk magnetization decreases, the poloidal velocity decreases as well, leading to an increase of the toroidal to poloidal velocity ratio. For a low disk magnetization, the Alfvén surface is located rather close to the disk surface. Because of the small poloidal velocity, the induction of the toroidal magnetic field (by the toroidal shear) is rather efficient, leading to a high toroidal to poloidal magnetic field ratio.

The excess of the magnetic energy stored in the toroidal magnetic field component, together with the smaller angular momentum loss rate result in an outflow

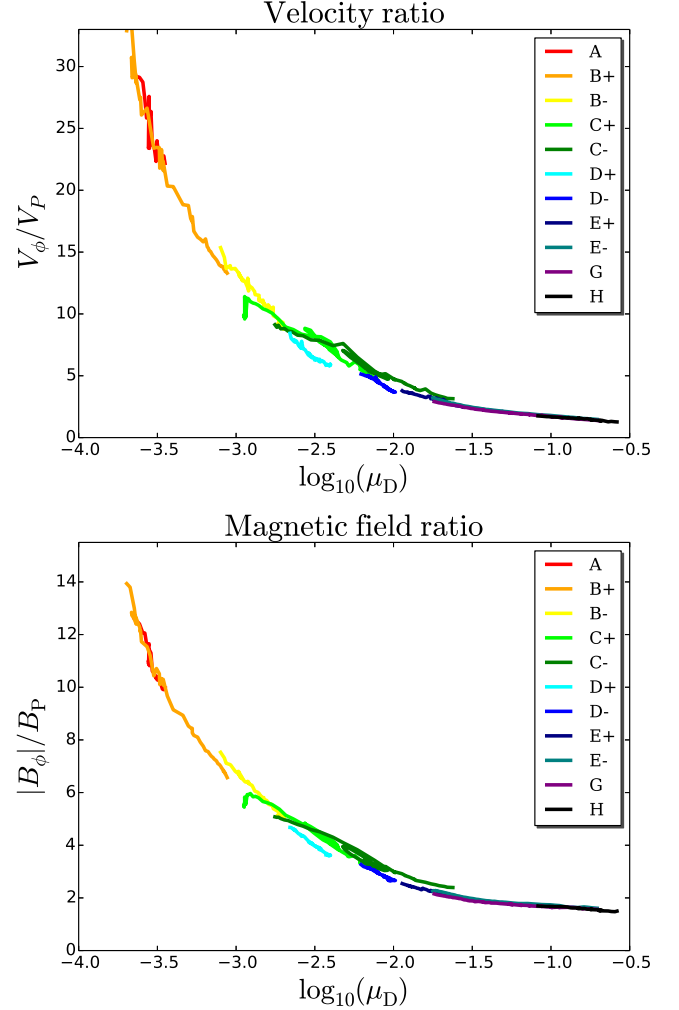


**Figure 11.** Ratio of the toroidal to poloidal components of the velocity (top) and the magnetic field (bottom), measured at the Alfvén point, with respect to the disk magnetization  $\mu_D$ . Each line represents the evolution of a single simulation (see Table 1) from 700 to 10,000 time units.

that is driven predominantly by the toroidal magnetic field pressure gradient, and not magneto-centrifugally. This regime of jet launching is usually known as producing “tower jets”. In the case of strong disk magnetization, the poloidal field dominates the toroidal magnetic field, while the extraction of disk angular momentum extraction is more efficient. As a consequence, the Alfvén lever arm is larger, and the mass loading is lower. This is the regime of the Blandford-Payne magneto-centrifugal launching.

The transition between the two regimes may appear smooth. Naturally, further details may depend on the diffusivity prescription that is applied. The ability of the disk to launch and sustain *tower jets* relies on its ability to generate a strong *toroidal* magnetic field component. However, in the standard approach, the diffusivity is parameterized only by the poloidal component of the magnetic field. On the other hand, a magnetic diffusivity prescription that considers both magnetic field components (as in Stepanovs et al. 2014) is able to suppress some of the launching regimes.

It is interesting to compare Fig. 11 to previous studies.

Casse & Ferreira (2000) have found in self-similar studies of jet launching that the quantities plotted in Fig. 11 follow certain interrelations. That is

$$\left[\frac{B_\phi}{B_P}\right]_A = -g_A \omega_A, \quad \left[\frac{v_\phi}{v_P}\right]_A = (1 - g_A) \omega_A, \quad (22)$$

where  $g \equiv 1 - \Omega/\Omega_F$  and the so-called fastness parameter  $\omega_A = \Omega_F r_A / V_{Ap,A}$  with the poloidal Alfvén speed at the Alfvén point  $r_A$ . For a low magnetization  $\mu_D \simeq 10^{-3.5}$  we derive from our data  $g_A \simeq 1/3$  and  $\omega_A \simeq 36$ , while for a high magnetization  $\mu_D \simeq 10^{-1}$  we derive from our data  $g_A \simeq 1/3.5$  and  $\omega_A \simeq 14$ . These number values, derived from our simulations (Fig. 11) and using the equations 22 are consistent with a direct estimate of the fastness parameter, i.e. applying  $\Omega_F \simeq 0.9$  at the foot point of the field line, and an Alfvén radius of  $r \simeq 1.8 - 2.6$ , resulting in  $\omega_A \simeq 15 - 20$ . Note that these values of the fastness parameter are on a different parameter range compared to the case of the self-similar studies resulting in  $\omega_A \simeq 1 - 2$  Casse & Ferreira (2000). We believe that this is mainly due to the fact that our study is *not* self-similar. The flux surfaces we investigate are the most innermost ones routed in the disk, thus deviating most from a self-similar structure. Also, collimation in our non-self-similar case is more rapid, resulting in a relatively small lever arm and an Alfvén radius only at  $r \simeq 1.8 - 2.6$ . Since the strong collimation, the acceleration is less efficient, resulting in a rather low velocity at the Alfvén point. Also the asymptotic speed along this flux surface is lower than expected from self-similar studies.

Having above mainly discussed the *jet acceleration* mechanism, a remaining question is the actual *launching* mechanism of the outflow. It has been well demonstrated (Ferreira 1997; Zanni et al. 2007; Murphy et al. 2010; Sheikhezami et al. 2012) that the main driving force for lifting the disk material out of the disk into the outflow and thereby passing the sonic surface is the gas pressure gradient. The poloidal Lorentz force is negative, thus does suppress the vertical lifting of material below several disk pressure scale heights. We note that the jet material is not lifted directly from the disk mid-plane into the outflow. It is the material close to the disk surface that is lifted in the outflow (Ferreira 1997; Sheikhezami et al. 2012).

Note that we need to distinguish between the *launching* and the *acceleration* mechanism. While disk winds seem to be launched in general by the gas pressure gradient, the outflow acceleration mechanism is different for weakly or strongly magnetized outflow, respectively. As discussed above, weakly magnetized jets are mainly driven by the magnetic pressure gradient, while highly magnetized jets are mainly driven by the magneto-centrifugal acceleration (see also Sheikhezami et al. 2012, where jets of different plasma beta and diffusivity were studied).

We should point out a potential numerical bias for the launching mechanism. As discussed in Murphy et al. (2010), the strong gradient in density across the disk surface (note the initially Gaussian density and pressure profile in vertical direction) leads to a numerical flux of matter. This is in addition to the mass loading that is allowed by the physical magnetic diffusivity and is dependent on the forces in the surface layer. Since our

numerical resolution is higher than in the Murphy et al. paper<sup>13</sup>, we expect the numerical mass loading to be weaker, but still present. Note that we also observe a jump in entropy across the disk surface as discussed in Murphy et al. (2010). Due to our higher resolution this effect of numerical heating is smaller, but still present.

### 6.3. Comparison to other studies

We have already mentioned the works of Tzeferacos et al. (2009) and Murphy et al. (2010) who were first in studying the jet launching in particular with respect to the disk magnetization. We now want to compare our results to the key findings of Murphy et al. (2010). Our simulation time scale seems to be somewhat larger<sup>14</sup>, however we know from our much longer-lasting simulations (up 500,000 dynamical time steps) that the evolutionary state we investigate is indeed in steady state.

Arguably the most essential result from Murphy et al. (2010) is the finding that super-fast jets can be launched only from the very central disk area where the magnetization is strong enough. This is demonstrated in their Fig. 15 that shows the radial disk and jet magnetization profile along the launching surface<sup>15</sup> and claim that outside of about 5 inner disk radii the magnetization is too low to launch fast jets<sup>16</sup>. Let's assume that the magnetization profile in their Fig. 15 is actually plotted for the disk surface defined by  $V_r$  changing sign and the size of the jet launching area of the disk is indeed 5 inner disk radii. We now discuss our findings in the light of their result. In Figure 8 we show the 2D profiles of the disk-jet magnetization of our simulation E+ at times

<sup>13</sup> Murphy et al. apply a resolution of 1.3 cells per disk scale height  $h$  at the inner disk radius, assuming that  $h = 0.1r$ . For larger radii the resolution increases to e.g. 13 grid cells per  $h$  at  $r = 10$ . We apply a resolution of 8 grid cells per scale height  $H = \epsilon R$  for all disk radii.

<sup>14</sup> We mention a discrepancy within the Murphy et al. (2010) paper concerning the evolutionary time of their simulations. We adopt a time unit  $T_0 \equiv R_0/V_{K,0}$  that arises naturally in the dimensionless of MHD equations (see e.g. Oued & Pudritz 1997; Fendt & Čemeljić 2002; Zanni et al. 2007; Tzeferacos et al. 2009, 2013; Sheikhezami et al. 2012), and use as length unit the inner disk radius  $R_0$  and as velocity unit the Keplerian velocity at  $R_0$  (as also Murphy et al. do). Murphy et al. apply a vertical grid extension of  $840r_0$  claiming that this “ensures that the magnetized outflow never reaches the boundaries” (quotation). However, they also state simulation times of 950 in their (orbital) time units, thus  $2\pi 950T_0 \simeq 6000T_0$ . From their Fig. 4 we derive a jet speed  $V_{jet} \simeq V_{K,0} = 1.0$ . In their time units the jet crosses the whole grid by  $T_{cross} = 840R_0/V_{K,0} = 840T_0 = 134 \times 2\pi T_0$ . Within 950 of their time units the jet would propagate  $6000R_0$ , well beyond the grid boundary. Thus, there seems to be an inconsistency either in their claim of a grid boundary such far that the outflow does not reach it or in their claim of simulation run time. As the authors do not show a time series on the global grid, the outflow evolution cannot be compared directly with other simulations.

<sup>15</sup> We feel obliged to mention an inconsistency concerning this figure. While the authors define the disk surface in Sect. 3.1 in their paper as the surface where  $V_r$  changes sign (as we do), in their Fig 15 they plot  $\sigma^+$  that is defined in equation 29 in their paper at  $z = h$  (however, after equation 29 they state that  $\sigma^+$  is measured at the disk surface, implying, in contradiction to their earlier definition, that  $z = h$  is the disk surface).

<sup>16</sup> We note that a proper radial scale for the horizontal axis is not really provided, as only one label is shown for the radius tick-marks, and no inner radius for the plot is stated. Also it remains unclear whether a linear or log scale is applied for the horizontal axis.



$t = 1000$  and  $t = 10000$ , and likewise for simulation D+ at  $t = 10000$ . Simulation E+ starts with a magnetization parameter  $\mu_0 = 0.01$ . At  $t = 1000$  and  $t = 10,000$  the actual disk magnetization in the area between  $r = 1.1$  and  $r = 1.5$  (the launching area of the fast jet), has reached values of  $m\mu_D = 0.012$  and  $\mu_D = 0.049$ , respectively<sup>17</sup>. Simulation D+ is initially weaker magnetized, characterized by  $\mu_0 = 0.005$  and reaches a disk magnetization of only  $\mu_D = 0.00218$  at  $t = 10,000$  in the same launching area.

In Figure 8 we have further indicated the surface of jet launching, here defined as the surface where the poloidal velocity changes from accretion to ejection, thus where  $v_r$  changes sign. This surface where  $v_r = 0$  is indicated in the panels by a black line. We find that this surface is typically located along  $z(r) = 2H(r)$  in our case, thus two times higher than indicated by the equation 29 in Murphy et al. (2010), but similar to Fig. 1 in Murphy et al. (2010). In our figure we have also indicated the surface where  $\mu = 1.0$  (white line). This location is typically at altitudes somewhat higher than the launching surface, at  $z(r) \simeq 3H(r)$ .

Note that these surfaces follow a radial path throughout the panels in Fig. 8, that are subsets of the whole simulation domain extending till  $R = 1,500$  at  $t = 10,000$ . These subset also show an area of simulation that has definitely reach a quasi-steady state. Here is a maybe another difference to the Murphy et al. paper, from which it is not clear to us, whether those simulations have reached a quasi-steady state.

In our simulations we therefore observe the following situation. Jet launching - the transition from accretion to ejection - may happen for lower values of disk magnetization compared to Murphy et al. (2010) - in general the outflow is launched from a region area where  $\mu(r, z) \simeq 0.1$ . The magnetization increases rapidly with vertical height providing the energy reservoir for subsequent jet acceleration. We find an increase of magnetization by a factor of ten within  $\Delta z \simeq 1.0$  (from  $\mu = 0.1$  to  $\mu = 1.0$  from  $z(r) = 2H(r)$  to  $z = 3H(r)$ ).

This configuration in the jet launching region is general and does not alter substantially for the simulation runs we have investigated. However, we find that the simulations with higher disk magnetization also have a higher initial jet magnetization (see the disk corona magnetization in the middle and lower panels in Fig. 8), and thus generate a more energetic jet. We mention that we find similar results for a slightly altered magnetic diffusivity profile, although this issue deserves a closer investigation in the future. In Sheikhezami et al. (2012) we have thoroughly investigated the impact of the diffusivity profile and magnitude on the launching process.

We now come back to the finding of the Murphy et al. of a *radially* limited disk area for jet launching, derived from the local disk magnetization. This result was essentially obtained by evaluating the *radial disk magnetization profile* of one simulation run for a low disk magnetization. In our paper, however, we investigate properties of jets launched from the innermost disk, considering a number of simulation runs resulting in a broad range of

disk magnetization *in that area*. On the other hand, our results may be further extrapolated such, that if outflows are launched from different radii along the disk, the properties of these outflow layers change with the *local* disk magnetization at the outflow footpoint - as described by the interrelations we have found. In contrary to Murphy et al. we do not find a locally constrained disk area for jet launching. This is partly by purpose. In order to reach very long simulation times, for this paper we have chosen a certain setup for the disk magnetization - the so-called strong diffusivity model - developed previously by Stepanovs & Fendt (2014), that allows for a smooth and steady accretion for very long simulation times. In this approach the advection and diffusion of magnetic flux leads to a steady-state *radial* magnetization profile that is roughly constant (see Fig. 23 in Stepanovs & Fendt 2014). This is comparable to the magnetization profile of Tzeferacos et al. (2009), who impose a constant magnetization profile along the equator. Thus, an outflow is launched from all over the disk surface in this model.

Note that discussion above again underlines the importance of the magnetic diffusivity model that is not known from first principles (as probably provided by global disk models considering direct simulations of the MRI including also further physical effects such as resistivity or heating/cooling). Still, we think that we may safely accept general conclusions such as from Murphy et al. concerning the limited disk area of jet launching, or the interrelation derived in the present paper between the disk magnetization and the jet properties. As long as we have to make a choice about the magnetic diffusivity distribution applied, the exact number values, such as the area of jet launching or e.g. the actual value of mass loading will still depend on the disk diffusivity model.

We therefore consider both approaches - the one presented here and the one by Murphy et al. (2010) - as complementary.

The work by Tzeferacos et al. (2009) is in some sense similar to ours as imposing a constant magnetization along the disk mid plane initially. Thus, the values for the magnetization used should be directly comparable to our  $\mu_D$ . However, they do not discuss the time evolution of the magnetization, nor the vertical profile of it. The range of disk magnetizations applied is from 0.1 to 3.0, thus smaller, although they mention a highly unsteady evolution for two very low magnetization levels,  $\mu = 0.01$  and  $\mu = 0.001$ , with maximum wind velocities of 20% of the Keplerian speed at the footpoint. In our simulations we find correspondingly low outflows speeds although higher by a factor 3 for  $\mu = 0.001$ .

## 7. CONCLUSIONS

We have presented results of MHD simulations investigating the launching of jets from magnetically diffusive accretion disks.

In a previous paper (Stepanovs & Fendt 2014) we have presented test simulations of our setup in spherical coordinates. We had further demonstrated that the disk accretion, ejection and, in particular, the accretion-to-ejection ratio of the mass and energy fluxes strongly depend on the actual disk magnetization. In the present paper we have applied a novel approach and have studied the relation between the jet properties, i.e. mainly the steady state MHD integrals, and the underlying disk

<sup>17</sup> These two snapshots in time are therefore seen on different positions along the dark blue tracks denoting the evolution of run E+ in Figures 5, 9, 11.

properties, with emphasis on the disk magnetization  $\mu_D$ .

Our work extends the results previously published by Tzeferacos et al. (2009) and Murphy et al. (2010) by investigating a much larger parameter space for the disk magnetization.

While Murphy et al. (2010) investigate how jet launching is affected by the magnetization profile along the disk surface, we follow a complementary approach and concentrate on the innermost disk area investigating the properties of jets launched from there considering a broad range of actual disk magnetization of  $\mu_D = 10^{-3.5} \dots 10^{-0.7}$ . The disk magnetization at this jet launching area follows from a simulation of the global accretion-ejection dynamics, and considers a quasi steady state.

As our main result, in this paper we present a series of correlations between the actual values of the jet conserved MHD quantities, such as energy, angular momentum, lever arm, or jet rotation, and the disk magnetization. These correlations cover more than three orders of magnitude of the disk magnetization.

Although the actual number values of the physical quantities presented in our study may depend on further details of various model prescriptions (such as e.g. the magnetic diffusivity that itself is a result of the disk microphysics causing the turbulence), we believe that the relations we have obtained are robust in general, at least qualitatively. In particular, we have obtained the following results:

(1) We have established a set of correlations between the dynamical properties of the jet and the underlying accretion disk. In particular, we have shown how the four jet MHD integrals are connected to the underlying disk magnetization.

(2) In particular, a high disk magnetization results in i) a larger Alfvén lever arm of the jet, ii) a larger jet specific angular momentum and energy, iii) a lower mass loading parameter  $k$ , iv) a lower mass ejection to accretion ratio, v) a higher accretion Mach number, vi) a lower velocity and a lower ratio of the toroidal to poloidal magnetic field component at the Alfvén surface, vii) a higher asymptotic jet speed, viii) a lower jet angular velocity.

For a comparatively low disk magnetization, the opposite of i)-vii) is true, while jet angular velocity also decreases, having a peak at a magnetization that is close to the critical magnetization that is about 0.01 – 0.05 for our setup.

(3) While Murphy et al. (2010) previous papers find indication for a limited size of the jet launching area, as the jet and disk magnetization falls below a critical value at a certain radius, our simulation give a different result. For the wide range of disk magnetization we investigated for the inner disk area, we find outflows for all these magnetizations.

(4) The launching of the outflow, thus lifting the accreting material into the outflow is done by the disk vertical pressure gradient, in agreement with previous studies (Tzeferacos et al. 2009; Murphy et al. 2010; Sheikheezami et al. 2012).

(5) Having defined the disk surface as the surface where accretion turns into ejection, thus  $v_r = 0$ , we find that it is located roughly at two disk thermal scale

heights  $z(r) \simeq 2H_T(r)$ . At this position the magnetization is somewhat below unity. The magnetization increases rapidly above the disk surface, providing the energy source for jet acceleration.

(6) In agreement with our previous studies (see e.g. Sheikheezami et al. 2012), the correlations we find between the jet parameters and the disk magnetization suggest the existence of two acceleration mechanisms at work. The correlations we find between the jet dynamical parameters and the disk magnetization typically show a different slope for low and high disk magnetization. Also the relative magnetic field strength of the toroidal component increases with decreasing disk magnetization. We interpret that acceleration is predominantly by magnetic pressure gradient for weak disk magnetization and by magneto-centrifugal support in the case of strong magnetization. Between the two parameter regimes there is a smooth transition, however the above mentioned change in slope indicates a "critical" disk magnetization of  $\mu_D \simeq 0.01$  that separates the two regimes. The existence of these two regimes has been discussed by Ferreira (1997) considering the outflow ejection efficiency indices.

(7) Our results are obtained from simulations applying a well defined magnetic diffusivity distribution for which the vertical profile is kept constant in time, while the strength of diffusivity changes in time with disk magnetization. Our diffusivity model allows for smooth and continuous accretion for very long time scales (Stepanovs & Fendt 2014) and results in a disk magnetization that is about constant along the midplane, similar to Tzeferacos et al. (2009). When using a different scale height for the diffusivity profile we have not detected a substantial variation in the mass loading, although we know from our previous work (Sheikheezami et al. 2012) that insofar, different assumptions on the diffusivity profile, in particular a time evolution in the level of diffusivity (Murphy et al. 2010; Fendt & Sheikheezami 2013) may alter our numerical results. Also, numerical effects may play a role (Murphy et al. 2010), however they are difficult to quantify. However, while variations in the disk evolution can be expected by using a different diffusivity prescription, we believe that our general results are indeed robust and can be applied generally.

We hesitate to speculate what kind of jet sources may have weakly or strongly magnetized disk. The disk magnetization may depend on the source of the magnetic field (a field from a disk or stellar dynamo or advected from the ISM), and can be altered by diffusive, viscous and advective processes. At this point, numerical simulations of the local disk physics are essential for our understanding.

We thank Andrea Mignone and the PLUTO team for the possibility to use their code. We thank Rachid Ouyed for valuable comments on an earlier version of the manuscript. We acknowledge comments and suggestions by anonymous referees. Our simulations were performed on the THEO cluster of Max Planck Institute for Astronomy. This work was partly financed by the SFB 881 of the German science foundation DFG.

## REFERENCES

- Anderson, J. M., Li, Z.-Y., Krasnopolsky, R., & Blandford, R. D. 2003, *ApJ*, 590, L107

- Bai, X.-N. & Stone, J. M. 2013, *ApJ*, 767, 30
- Balbus, S. A. & Hawley, J. F. 1991, *ApJ*, 376, 214
- Blandford, R. D. & Payne, D. G. 1982, *MNRAS*, 199, 883
- Casse, F. & Ferreira, J. 2000, *A&A*, 353, 1115
- Casse, F. & Keppens, R. 2002, *ApJ*, 581, 988
- . 2004, *ApJ*, 601, 90
- Colella, P. & Woodward, P. R. 1984, *Journal of Computational Physics*, 54, 174
- Fendt, C. & Camenzind, M. 1996, *A&A*, 313, 591
- Fendt, C. & Ćemeljić, S. 2002, *A&A*, 395, 1045
- Fendt, C. & Sheikhnezami, S. 2013, *ApJ*, 774, 12
- Ferreira, J. 1997, *A&A*, 319, 340
- Ferreira, J. & Pelletier, G. 1995, *A&A*, 295, 807
- Foglizzo, T. & Tagger, M. 1995 *A&A*, 287, 297
- Fromang, S. 2013, in *EAS Publications Series*, Vol. 62, EAS Publications Series, 95–142
- Gressel, O. 2010, *MNRAS*, 405, 41
- Hawley, J. F., Fendt, C., Hardcastle, M., Nokhrina, E. & Tchekhovskoy, A. 2015, *Space Sci. Rev.* 191, 441
- Johansen, A. & Levin, Y. 2008, *A&A*, 490, 501
- Kato, S. X., Kudoh, T. & Shibata, K. 2002, *ApJ*, 565, 1035
- Königl, A. & Salmeron, R. 2011, *The Effects of Large-Scale Magnetic Fields on Disk Formation and Evolution*, ed. Garcia, P. J. V., 283–352
- Königl, A., Salmeron, R., & Wardle, M. 2010, *MNRAS*, 401, 479
- Kudoh, T., Matsumoto, R., & Shibata, K. 1998, *ApJ*, 508, 186
- Lesur, G. & Longaretti, P.-Y. 2009, *A&A*, 504, 309
- Li, Z. 1995, *ApJ*, 444, 848
- Londrillo, P. & del Zanna, L. 2004, *Journal of Computational Physics*, 195, 17
- Meliani, Z., Casse, F., & Sauty, C. 2006, *A&A*, 460, 1
- Mignone, A., Bodo, G., Massaglia, S., Matsakos, T., Tesileanu, O., Zanni, C., & Ferrari, A. 2007, *ApJS*, 170, 228
- Murphy, G. C., Ferreira, J., & Zanni, C. 2010, *A&A*, 512, A82
- Ouyed, R. & Pudritz, R. E. 1997, *ApJ*, 482, 712
- Pelletier, G. & Pudritz, R. E. 1992, *ApJ*, 394, 117
- Pudritz, R. E. & Norman, C. A. 1983, *ApJ*, 274, 677
- Pudritz, R. E., Ouyed, R., Fendt, C., & Brandenburg, A. 2007, *Protostars and Planets V*, 277
- Ray, T., Dougados, C., Bacciotti, F., Eisloffel, J. & Chrysostomou, A. 2007, *Protostars and Planets V*, 231
- Salmeron, R., Königl, A., & Wardle, M. 2011, *MNRAS*, 412, 1162
- Shakura, N. I. & Sunyaev, R. A. 1973, *A&A*, 24, 337
- Sheikhnezami, S., Fendt, C., Porth, O., Vaidya, B., & Ghanbari, J. 2012, *ApJ*, 757, 65
- Sheikhnezami, S. & Fendt, C. 2015, *ApJ*, 814, 113
- Stepanovs, D. & Fendt, C. 2014, *ApJ*, 793, 31
- Stepanovs, D., Fendt, C. & Sheikhnezami, S. 2014, *ApJ*, 796, 29
- Tzeferacos, P., Ferrari, A., Mignone, A., Zanni, C., Bodo, G. & Massaglia, S. 2009, *MNRAS*, 400, 820
- . 2013, *MNRAS*, 428, 3151
- Uchida, Y., & Shibata, K. 1984, *PASJ*, 36, 105
- Uchida, Y., & Shibata, K. 1985, *PASJ*, 37, 515
- Ustyugova, G. V., Koldoba, A. V., Romanova, M. M., Chechetkin, V. M., & Lovelace, R. V. E. 1995, *ApJ*, 439, L39
- Ustyugova, G. V., Koldoba, A. V., Romanova, M. M., Chechetkin, V. M., & Lovelace, R. V. E. 1999, *ApJ*, 516, 221
- Wardle, M. & Königl, A. 1993, *ApJ*, 410, 218
- Zanni, C., Ferrari, A., Rosner, R., Bodo, G., & Massaglia, S. 2007, *A&A*, 469, 811

# Alfven lever arm squared

